TRIUMF

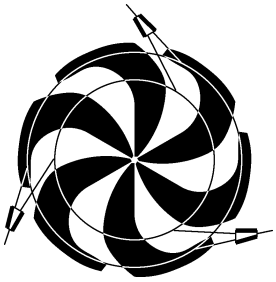

ANNUAL REPORT
SCIENTIFIC ACTIVITIES
1997

CANADA'S NATIONAL MESON FACILITY
OPERATED AS A JOINT VENTURE BY:

UNIVERSITY OF ALBERTA
SIMON FRASER UNIVERSITY
UNIVERSITY OF VICTORIA
UNIVERSITY OF BRITISH COLUMBIA

ASSOCIATE MEMBERS:

UNIVERSITY OF MANITOBA
UNIVERSITÉ DE MONTRÉAL
UNIVERSITY OF REGINA
UNIVERSITY OF TORONTO

UNDER A CONTRIBUTION FROM THE
NATIONAL RESEARCH COUNCIL OF CANADA

APRIL 1998

The contributions on individual experiments in this report are outlines intended to demonstrate the extent of scientific activity at TRIUMF during the past year. The outlines are not publications and often contain preliminary results not intended, or not yet ready, for publication. Material from these reports should not be reproduced or quoted without permission from the authors.

Experiment 684
μSR spin relaxation studies of small molecules in the gas phase
(J. Pan, D. Fleming, UBC–TRIUMF)

This experiment studies the muon spin relaxation in some simple gas phase systems with the primary goal of measuring the chemical reaction rates. This year, the focus of our research is on the Mu+NO reaction with different moderators (He, N_2 and CH_4) in both longitudinal (LF) and transverse (TF) magnetic fields. One particular goal is to understand and resolve the inconsistency in the data reported in the 1996 Annual Report.

One week of experiments was carried out on M15 in the LF at pressures less than 60 atm and room temperature. The result indicated that our earlier data obtained on M9 in high pressure He and CH_4 moderators (see 1996 Annual Report) were indeed compromised, most likely due to impurities in the CH_4 gas used at that time. Note that in the He experiment, a small amount of some other moderator is required to produce Mu. CH_4 had been used previously and hence the previous He results are also unreliable. Apart from the impurity problem, the new data also showed that the amount of CH_4 added was large enough to affect the relaxation rate in He (hence some other gas must be used instead, see below). More importantly, though, the new data gave consistent results for all three moderator gases (He, N_2 and CH_4): the spin exchange rate constants are similar in all three moderators and consistent with previous measurements in N_2 moderator; the chemical rate constant in N_2 agrees with our earlier results and the rate constants are increasingly larger in the order of moderators given above (see Fig. 47).

Data were also obtained on M9 in both TF and LF at room temperature but pressures up to 500 atm. In the past, this reaction has always been studied in LF in order to separate the contribution from chemical reaction and spin exchange, taking advantage of the fact that the chemical rate is not field dependent but the apparent spin flip rate is. This separation can, however, also be effected in TF for the following two reasons: first, the contribution from spin exchange depends on the field strength but the chemical reaction does not; secondly, the chemical reaction depends on the moderator (both its pressure and its collisional efficiency) but the spin exchange does not. The measurements were done by varying both field strength and total pressures in moderators He, N_2 and CH_4. In He, $\sim$ 1 atm N_2 or Xe were added as the third dopant gas to produce Mu. For comparison purposes, relaxation rates were also measured in LF with the same gas mixture in some cases. The following conclusions can be drawn from the data: a) the TF results are entirely consistent with the LF data; b) with the range of pressure variation we have now, weak TF (< 8 G) measurements give as good, if not better, results as LF measurements (see Fig. 47); c) of all the third dopant gases we have tried, Xe gave the best results for forming Mu in He and yet did not introduce any additional relaxation.

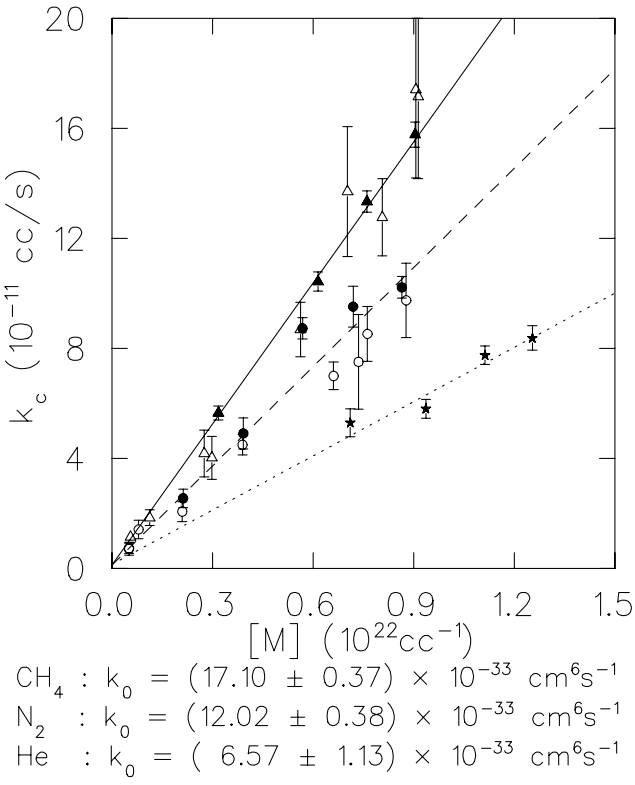

Fig. 47. Bimolecular rate constants for the Mu+NO+M reaction. The solid points are TF data and the hollow points are LF data.

Figure 47 shows all of the data we have obtained so far, including measurements in both TF and LF, on both M9 and M15. In all three moderators, the addition reaction is still in the low pressure regime. The corresponding termolecular rate constants are also shown in the figure. Our extracted rate constants are now much more precise and probably more precise than the H atom data, facilitating an important comparison with theory. The moderator dependence we have established in the low pressure (termolecular) limit, with $k_0^{CH_4} > k_0^{N_2} > k_0^{He}$, is consistent with established trends in the literature for analogous and/or similar H atom reactions, but this is the *first* time it has been established for unimolecular dissociation in Mu reactivity.

Attempts to measure the reaction rate at lower temperatures (−150 K) were not successful. Although the target vessel and the basic technique have been working fine, the gas handling and mixing technique have to be improved in order to achieve reliable results at such low temperatures.

Experiment 687
μSR in frustrated antiferromagnetic pyrochlores $A_2B_2O_7$
(S.R. Dunsiger, UBC; B.D. Gaulin, McMaster; R.F. Kiefl, UBC)

In systems where magnetic ions occupy the vertices of edge or corner sharing triangular units, there is no spin configuration which simultaneously satifies all the magnetic couplings, if all these interactions are antiferromagnetic. Stacked triangular, Kagomé, fcc, and pyrochlore lattices are all examples of this *geometric* frustration. The purpose of Expt. 687 is to apply μSR to further our understanding of the effect of this frustration on the ground state and low lying magnetic excitations in the pyrochlores $A_2B_2O_7$, where magnetic ions form a network of corner sharing tetrahedra.

A system of Heisenberg spins interacting via nearest-neighbour antiferromagnetic couplings on the pyrochlore lattice displays a classical ground state with macroscopic degeneracy, since the lowest energy spin configuration requires only that $\Sigma_{i=1}^{4}\mathbf{S}_i = 0$ for each tetrahedron. This feature led Villain to argue that these systems remain in a *cooperative paramagnetic* state with only short range spin-spin correlations for all T>0 [Z. Phys. **B33**, 31 (1979)] and this has been confirmed by Monte Carlo simulations [Reimers, Phys. Rev. **B45**, 7287 (1992)]. However, additional factors such as magnetic anisotropy, further nearest neighbour exchange and fluctuations [Bramwell *et al.*, J. Appl. Phys. **75**, 5523 (1994)] can lift the degeneracy and lead to Néel order involving complicated canted structures, as observed in $Nd_2Mo_2O_7$ [Greedan *et al.*, Phys. Rev. **B43**, 5682 (1991)] and possibly other more exotic ground states.

The present work was motivated by neutron scattering results by Gaulin *et al.* on the pyrochlore oxide $Tb_2Mo_2O_7$ [Z. Tun, Phys. Rev. Lett. **69**, 3244 (1992)] which shows evidence for short range order and a partial freezing of the Tb^{3+} moments as one approaches the ordering temperature $T_F = 25$ K from above. The results suggested the ground state was a type of dense spin glass.

We have previously carried out measurements of the muon $1/T_1$ spin relaxation rate in the pyrochlores $Y_2Mo_{2-x}Ti_xO_7$ (x=0, 0.4, 0.8, 1), as illustrated in Fig. 48. At high temperatures one is in the motionally narrowed limit, where the spin fluctuation rate of the Mo^{4+} moments is much faster than the Larmor

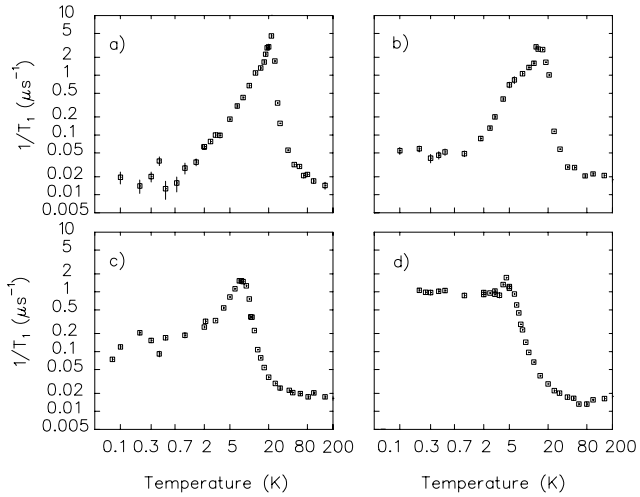

Fig. 48. Relaxation rate of muon spin polarization in a) $Y_2Mo_2O_7$, b) $Y_2Mo_{1.6}Ti_{0.4}O_7$, c) $Y_2Mo_{1.2}Ti_{0.8}O_7$ and Y_2MoTiO_7 in an applied field H = 0.02 T.

frequency of the muon. The sharp rise in the average $1/T_1$ as the temperature is reduced is attributed to critical slowing down of the Mo^{4+} fluctuations. A large static internal magnetic field with a very broad distribution develops below a spin freezing temperature T_F, such that no coherent muon spin precession is observed. Hence these materials show behaviour reminiscent of conventional spin glasses. However, the most remarkable feature in the data is the presence of a sizeable residual spin relaxation rate at low temperatures. This is evidence for a non-zero peak in the density of magnetic excitations near zero energy. The nature of these low temperature excitations is not yet understood. It is possible that they are "remnants" of a dispersionless spin-wave branch ("zero-modes") predicted theoretically for nearest-neighbour Heisenberg spins on a pyrochlore lattice [Reimers *et al.*, Phys. Rev. **B43**, 865 (1991); Harris *et al.*, Phys. Rev. **B45**, 7536 (1992); Reimers and Berlinsky, Phys. Rev. **B48**, 9539 (1991)].

The addition of diamagnetic Ti^{4+} ions as substitutional impurities on the B site introduces random disorder into these systems. The muon spin depolarization rate is roughly temperature independent below 1 K, at values which increase with increasing impurity concentration.

There has been some question as to the possible role of oxygen vacancies present below the 1% level introducing random disorder and hence giving rise to $1/T_1$ spin relaxation. While the precise extent of the oxygen deficiency has still to be determined by chemical analysis, a deoxygenated sample of $Y_2Mo_2O_7$ has now been examined. As shown in Fig. 49, this source of disorder appears to have at most a minor role in determining the low temperature spin dynamics.

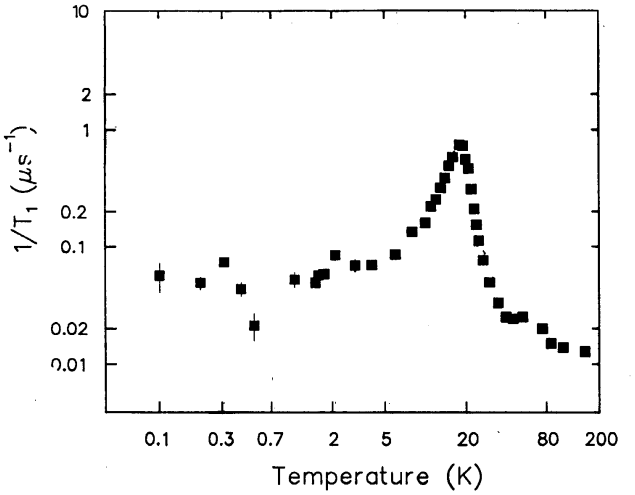

Fig. 49. Relaxation rate of muon spin polarization in $Y_2Mo_2O_{7-\delta}$ in an applied field H = 0.02 T.

The Mo^{4+} ion is the sole magnetic species in $Y_2Mo_{2-x}Ti_xO_7$, located on the B site. We have also studied $Tb_2Ti_2O_7$, where the A site alone is populated by a magnetic ion. The results are shown in Fig. 50. There is no indication of any phase transition, as evidenced by cusps or sharp discontinuities in $1/T_1$ and $Tb_2Ti_2O_7$ remains paramagnetic, even at temperatures in the mK range. Elastic neutron scattering measurements reveal diffuse peaks at ∼1 and 3 A^{-1} which increase in intensity as the temperature is reduced below 50 K, but which are *not* resolution limited. These peaks are evidence for the development of short range correlations over the lengthscale of a single tetrahedron (see Fig. 51).

Using inelastic neutron scattering, a diffuse peak has also been observed below 100 K at 0.38 THz energy transfer. The position of this peak is independent of wave vector, as can be seen in Fig. 52. The

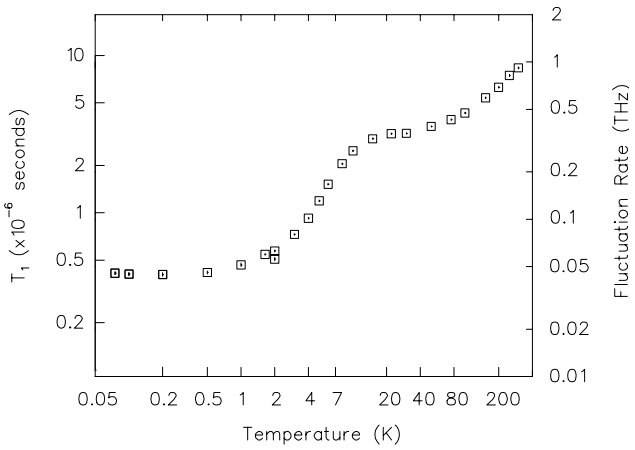

Fig. 50. The variation with temperature of the muon spin relaxation time T_1 and corresponding Tb^{3+} moment fluctuation rates are shown for $Tb_2Ti_2O_7$ in a longitudinally applied field of 0.005 T.

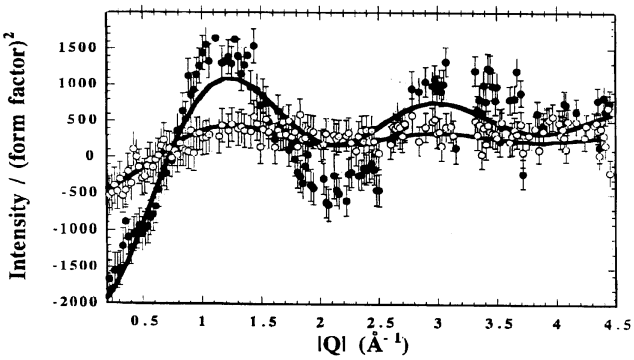

Fig. 51. The difference between diffraction patterns taken at i) 2.5 K and ii) 50 K and that taken at 100 K, corrected for the Tb^{3+} magnetic form factor, is shown. The solid lines are fits of the net intensity data set to the scattering expected from spins correlated over a single tetrahedron only, and taking up the local structure displayed by FeF_3.

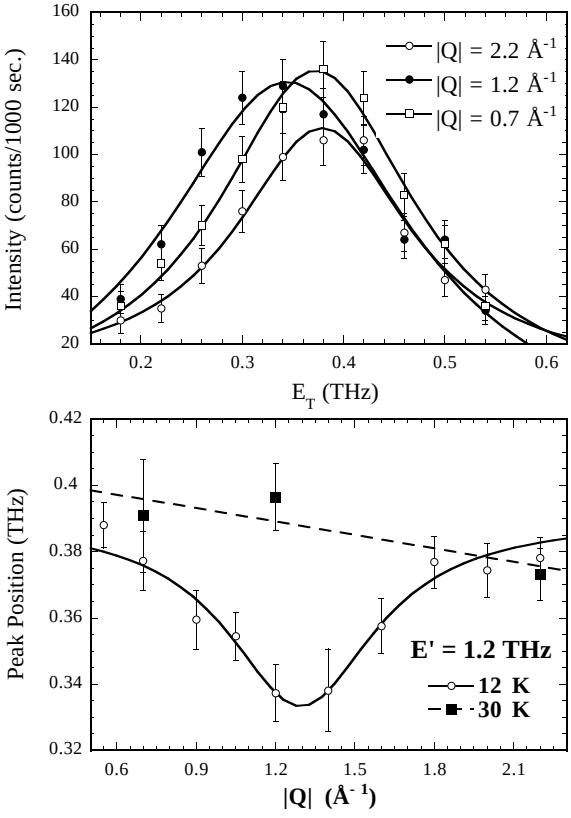

Fig. 52. Top panel: Constant |Q| scans at 0.7, 1.2, and 2.2 $Å^{-1}$ at T=12 K are shown. The inelastic peak at 1.2 $Å^{-1}$ is centered at a lower energy than those at 0.7 or 2.2 $Å^{-1}$. Bottom panel: The dispersion of the magnetic excitation spectrum at 12 K and 30 K is shown. At 12 K a clear incomplete softening of the modes is seen near the first maximum in the magnetic structure factor (see Fig. 50)

resulting gap in the excitation spectrum is thought to be due to the the highly anisotropic nature of the Tb^{3+} ion, which has a large orbital contribution to its angular momentum in its $^7F_6$ ground state. Below 30 K there is a softening of this dispersionless mode, which may indicate the development of a localized magnetic excitation, with features reminiscent of a "spin roton" [Chandra and Coleman, Int. J. Mod. Phys. **B3**, 1729 (1989)].

The increase in $1/T_1$ below 18 K occurs at a temperature comparable with the measured gap energy. In longitudinal field experiments in the "motionally narrowed" limit of rapid spin fluctuations

$$1/T_1 = \frac{2\Delta^2\nu}{\nu^2 + \nu_L^2}$$

where $\Delta = \gamma_\mu B$ is the gyromagnetic ratio of the muon ($2\pi \times 135.54\,(10^6$ rads s^{-1} tesla^{-1})) times the rms internal magnetic field B. ν is the fluctuation rate of the internal field and $\nu_L = \gamma_\mu B_{\rm ext}$ is the frequency of the muon in the external magnetic field. Hence the increase in the muon spin relaxation rate corresponds to a decrease in the Tb^{3+} ion fluctuation rate. This is reasonable, since there are a decreased number of accessible states as the temperature falls below the anisotropy gap. At lower temperatures the fluctuations are attributed to a collective tumbling of spins correlated over a single tetrahedron.

By contrast, the Gd^{3+} ion has a $^8S_{7/2}$ ground and hence no orbital contribution to its angular momentum. As can be seen in Fig. 53, $1/T_1$ is roughly temperature independent above 4 K. The upturn at lower temperatures is consistent with magnetic specific heat measurements [Raju, unpublished], which indicate a broad peak at 2 K and a phase transition at 1 K.

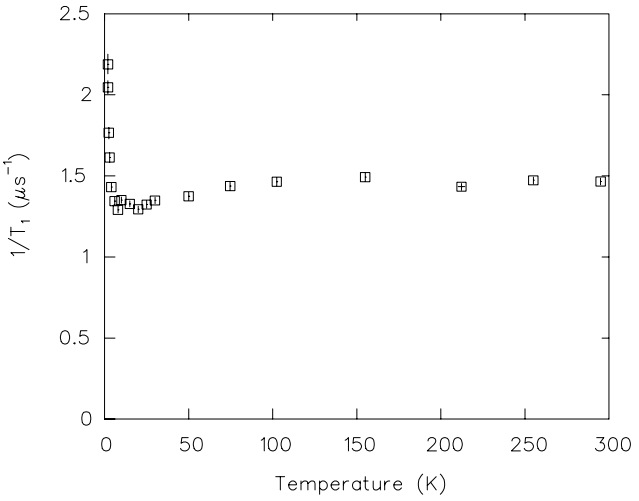

Fig. 53. Relaxation rate of muon spin polarization in $Gd_2Ti_2O_7$ in an applied field H = 0.005 T.

The garnet $Gd_3Ga_5O_{12}$ (GGG) is made up of Gd ions which are situated on two interpenetrating corner sharing triangular lattices. Since the exchange interactions are almost purely antiferromagnetic, this material is also thought to be geometrically frustrated. Like the oxide pyrochlores, it can be synthesized to produce samples of exceptional purity and very low disorder.

Magnetic susceptibility and specific heat measurements indicate a spin glass state below ∼200 mK, an antiferromagnetic ordering transition as the external field is increased to ∼1 T and a return to paramagnetism at somewhat higher field [Schiffer *et al.*, Phys. Rev. Lett. **73**, 2500 (1994)]. In June, 1996 μSR $1/T_1$ measurements in a longitudinally applied field of 0.005 T were made on GGG to try and confirm the behaviour reported. The results were not conclusive but no evidence for a phase transition was observed. This summer we repeated the experiment, on this occasion using

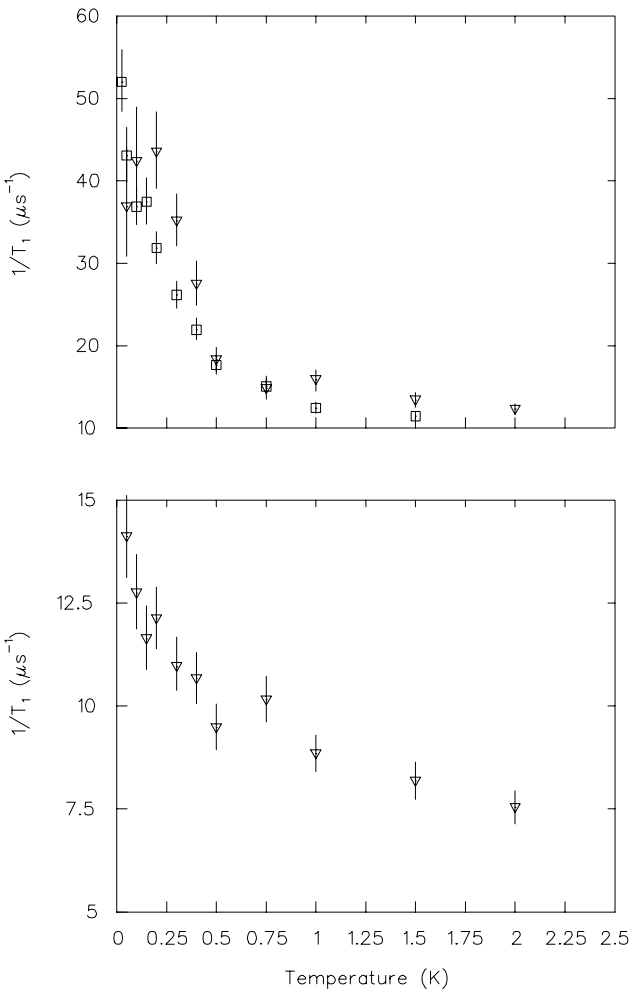

Fig. 54. Relaxation rate of muon spin polarization in gadolinium gallium garnet in applied magnetic fields of 0.001 T (top) and 1 T (bottom) as a function of temperature. The squares indicate measurements taken on a powder sample, the triangles measurements on a 111 single crystal.

a single crystal with the (111) direction parallel to applied magnetic fields. As shown in Fig. 54, there is again no marked evidence for a transition to a spin glass phase in low field, as would be indicated by a cusp in $1/T_1$ at the freezing temperature (see Fig. 48a). Nor is any transition to long range order observed at 1 T. The Gd moments continue to fluctuate even at 50 mK. The results of measurements of the paramagnetic shift, a measure of the local susceptibility, are shown in Fig. 55. While the temperature dependence is Curie-like above ∼2 K, there is a crossover at lower temperatures. Thus the system is no longer well described as a simple paramagnet and indicates the onset of short range correlations.

The μSR results are consistent with recent neutron scattering experiments by Petrenko *et al.* [unpublished]. Their measurements on a powder sample indicate that there is a continuous build up of magnetic correlations below 2.9 K, as evidenced by diffuse peaks and a liquid-like structure factor. At 140 mK sharper peaks appear which increase in intensity as the temperature is further reduced, but which remain broader than the resolution limit of the spectrometer. These peaks are attributed to Gd ions correlated over 30 $\AA$.

A variety of geometrically frustrated systems [Ramirez, Ann. Rev. Mat. Sci. **24**, 453 (1994); Schiffer and Ramirez, Comments Cond. Mat. Phys. **18**, 21 (1996)] show evidence for persistant fluctuations at low temperatures. However, the dynamical properties of more conventional random spin systems, which are frustrated instead due to bond or site disorder, are still far from being understood. In November of this year measurements of $1/T_1$ were undertaken on AuFe (0.5%), a "classic" spin glass with a transition at ∼5 K. As shown in Fig. 56, the spectra at the lowest

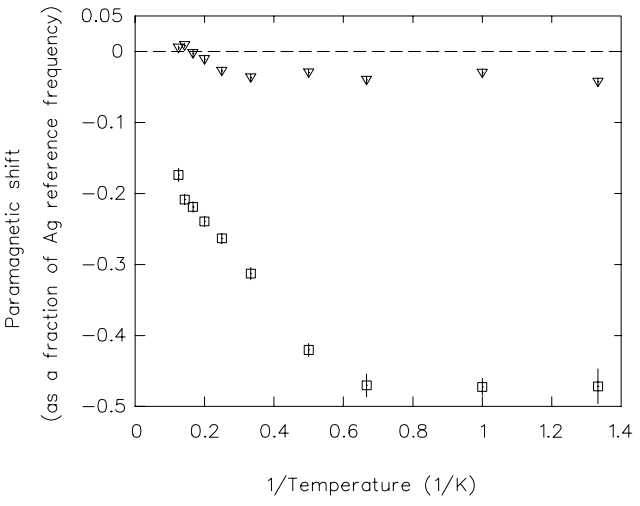

Fig. 55. Paramagnetic shift of muon spin precession frequency in gadolinium gallium garnet in an applied magnetic field of 0.1 T as a function of temperature.

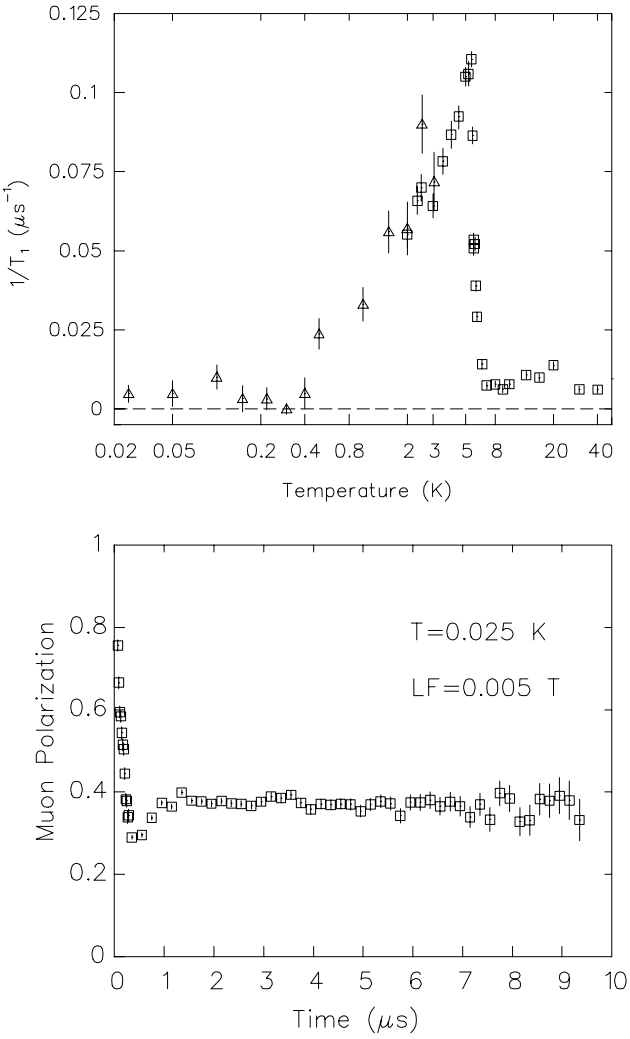

Fig. 56. Top panel: Relaxation rate of muon spin polarization in AuFe in an applied magnetic field of 0.005 T. Bottom panel: Typical muon spin relaxation function in AuFe at 25 mK.

temperatures explored were characteristic of a system of random *static* moments described by a Kubo-Toyabe function. Within the resolution limits of the μSR technique, $1/T_1 \rightarrow 0$ below $0.1T_F$ (see top panel of Fig. 56), in contrast with the pyrochlores. This would seem to confirm that there are distinct excitations present in the latter geometrically frustrated systems, not observed in more conventional metallic ones.

Experiment 713
Muonium chemistry in supercritical water
(P.W. Percival, SFU)

The properties of water change markedly when it is subjected to temperatures and pressures near or above the critical point (374°C, 220 atm). The ionic product falls by many orders of magnitude and the dielectric

constant is reduced to values typical of organic solvents. It is even possible to sustain a flame by injecting oxygen into a supercritical aqueous solution of an organic material.

The ability to modify the macroscopic properties of water and other supercritical fluids by changing temperature and pressure has led to a variety of industrial applications, including precision cleaning, extraction, separations, crystallization, and chemical synthesis. More recently, attention has been directed to the possibility of waste destruction by supercritical water oxidation (SCWO). Proposed applications range from water recycling in spacecraft life support systems to clean-up of old nuclear processing facilities (e.g. the Hanford site in Washington State).

A significant hurdle to practical development of SCWO destruction facilities is the current lack of detailed knowledge of physical, chemical and transport properties of supercritical fluids at the molecular level, particularly free radical chemistry and kinetics under such conditions. Experiment 713 is designed to probe SCW chemistry by μSR, using muonium as a model for the hydrogen atom. It is expected to provide information on changes to solvent structure, reaction kinetics and free radical chemistry (by studying muonium adducts of alkenes and aromatics).

Muonium in pure water

The variation of muon signal amplitudes as a function of temperature and pressure in water was reported last year [Expt. 713, 1996 Annual Report, p. 54]. The data fall on smooth curves when plotted against fluid density. There is a large increase in the muonium fraction at low density, consistent with the modification of water properties from liquid to gas-like, as the density falls. However, there is also a minimum in the intermediate, sub-critical region, where water is still a dense liquid.

This year the muonium hyperfine constant (hfc) was determined over a wide range of conditions and also found to depend primarily on density (see Fig. 57). There is an obvious trend at low densities towards the hfc of muonium in vacuum (4463 MHz), as expected for a low pressure gas. The trend is less clear at high density, and there may even be a minimum around 0.9 g cm^{-3}, as found for the muonium amplitude. Unfortunately the muonium signals are very weak in this region and long data acquisition times are necessary to make precise determinations. A smooth variation of hfc with density suggests a model in which muonium resides in a "bubble" in a continuous medium, with the electronic wave function subject to solvent pressure. This is consistent with the hydrophobic nature of the hydrogen atom, and molecular dynamics calculations of Mu and H in transient clathrate-like

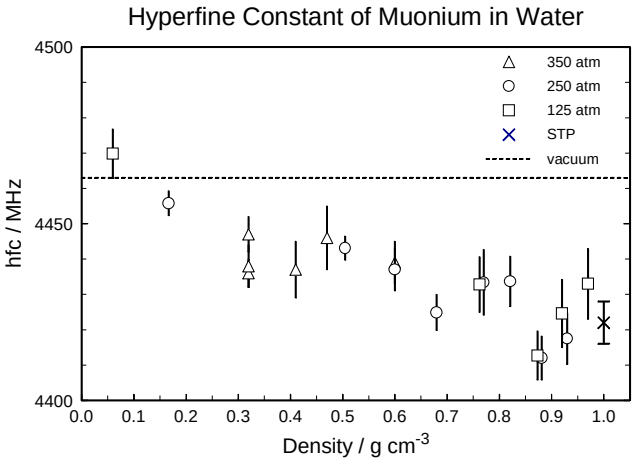

Fig. 57. Muonium hyperfine constant as a function of density in pure water.

cages in water [Klein *et al.*, J. Phys. Chem. **87**, 5055 (1983); J. Chem. Phys. **80**, 5718 (1984)]. Precise measurements of the H atom hfc recently revealed a negative temperature dependence at 1 atm [Roduner *et al.*, J. Chem. Phys. **102**, 5989 (1995)] (i.e. the hfc falls as the density is reduced). This result, and the measured isotope dependence can be explained by a combination of solvent pressure and spin delocalization onto solvent molecules. However, the existence of a solvent cage depends on hydrogen bonding between water molecules, which could be drastically altered by the extreme conditions of SCW. Alternatively water molecules may cluster around H atoms to low pressures. Our hfc data provide the means to test theories and computational models as they are developed.

Muonium kinetics in aqueous solutions

Since muonium has only a slow relaxation rate (λ_0) in pure water, even under SCW conditions, it is clear that it does not react with this solvent at a significant rate, making it possible to study reactions with solutes. The usual procedure is to study the decay rate (λ) as a function of reactant concentration ([X]) and determine the second-order rate constant (k_{M}) from the relation

$$\lambda = \lambda_0 + k_{\mathrm{M}}\,[\mathrm{X}]\ .$$

However, for practical reasons a single concentration is studied under different temperatures and pressures in the SCW cell. Furthermore, the reactant concentration varies as the solution density (ρ) changes. Thus the rate constant is calculated from

$$k_{\mathrm{M}} = \frac{(\lambda - \lambda_0)}{[\mathrm{X}]} \cdot \frac{\rho(298\ \mathrm{K}, 1\ \mathrm{atm})}{\rho(T,P)}\ .$$

The only reaction studied to date is spin exchange between muonium and nickel(II). It was chosen as a representative diffusion-limited rate process. Some of the

results are plotted as a function of temperature at fixed pressure in Fig. 58. There is a discrepancy between the data sets from two different run periods which can not be fully explained at this time. A plausible hypothesis is that the concentration of paramagnetic Ni(II) fell with time in the second period (open circles in Fig. 58) due to a redox reaction with a trace contaminant (organic solvent used for cleaning). In any event there is no doubt that the rate constant rises with temperature at a rate much less than that predicted by simple diffusion theory (proportional to viscosity/temperature, η/T). Furthermore the sudden drop in k in the supercritical region is also definite. It suggests a drastic change in the water structure and thence diffusion rates. This was explored by a study of the pressure dependence at various fixed temperatures. The effect is greatest at temperatures close to the critical point, where the effective activation volume

$$\Delta V^{\ddagger} = -RT \left(\frac{\partial \ln k}{\partial P} \right)_T$$

is negative and very large (of order –300 cm^3 mol^{-1} as indicated by the dashed line in Fig. 59). In contrast, the activation volume for a diffusion limited reaction of muonium at room temperature was found to be +3 cm^3 mol^{-1} [Brodovitch *et al.*, Radiat. Phys. Chem. **3**, 105 (1988)], similar to H. Further experiments will be necessary to determine whether the large effect is due to the supercritical conditions or is related to spin exchange.

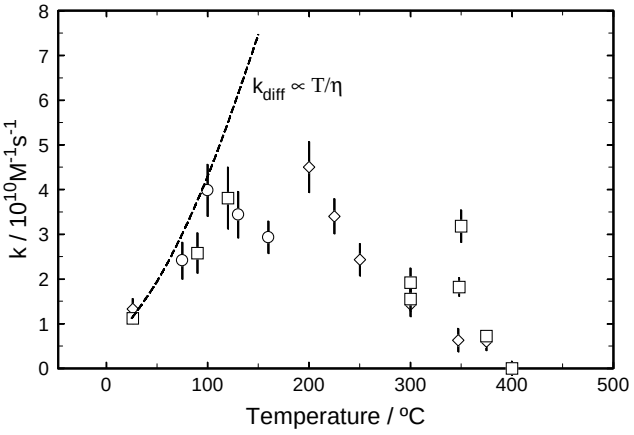

Fig. 58. Rate constants for Mu + Ni(II) spin exchange at 250 atm.

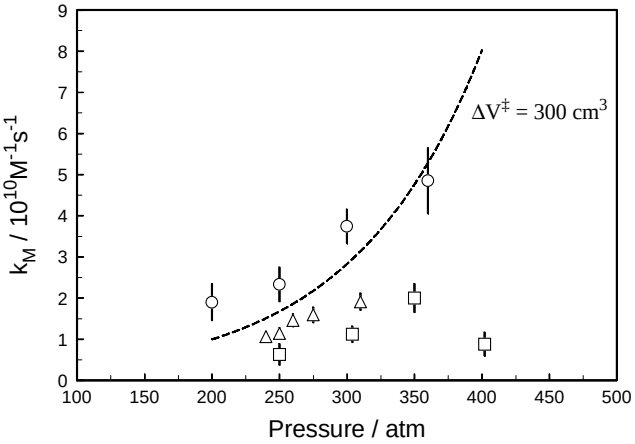

Fig. 59. Pressure dependence of the Mu + Ni(II) rate constant for temperatures in the range 350 – 375°C.

Experiment 742
Scattering of muonic hydrogen isotopes
(V.M. Bystritsky, JINR, Russia; R. Jacot-Guillarmod, F. Mulhauser, Fribourg; J. Wozniak, Cracow)

The scattering processes of μd and μt atoms in hydrogen via reactions

$$\mu d + \mathrm{H}_2 \rightarrow \mu d + \mathrm{H}_2,$$
$$\mu t + \mathrm{H}_2 \rightarrow \mu t + \mathrm{H}_2,$$

present clear evidence for the Ramsauer-Townsend effect. This effect makes the scattering cross section extremely small ($\sim 10^{-21}$ cm^2) at collision energies of $2 - 20$ eV. The consequence is a quasi transparency of the protium for μd and μt atoms.

In February, 1996, measurements were made with beams of μd atoms emitted into vacuum and reaching the downstream foil (more details about apparatus in [Knowles *et al.*, Nucl. Instrum. Methods **A368**, 604 (1996)]), covered by layers of neon and different thicknesses of protium, frozen at 3 K. The measurements are clear observations of the Ramsauer-Townsend effect. However, we observed that solid state effects are not negligible in this type of experiment. The characteristic thermalization time of the muonic atoms is fairly similar in solid and gaseous hydrogen. The major solid state effect is the existence of the Bragg cut-off energy limit, which excludes a deep thermalization to occur in solid hydrogen. In consequence, there is an enhancement of the hydrogen transparency for the μp atoms. Therefore, we observed some early time events due to muons stopping in the downstream protium layer, producing μp atoms which drift to the adjacent neon layer.

In January, 1997, we started to study the solid state effects in the μt and μp scattering process in H_2. We deposited a neon layer on top of pure protium located on the upstream foil. The μp atoms were formed in the protium layer; a certain portion of those atoms reach

the adjacent layer and transfer their muon to the neon. The bottom graph of Fig. 60 shows the resulting neon time spectrum. There are clear evidences for such a process. The slope of the time spectrum for time between 0 and 0.5 μs is characteristic of the scattering processes $\mu p + H_2 \rightarrow \mu p + H_2$.

The Ramsauer-Townsend effect was then studied with beams of μt atoms. The top graph of Fig. 60 shows the neon time spectrum following the muon transfer to neon. The events from 0.3 to 1.5 μs are due to μt which were emitted from the upstream layer (mixture of protium and small amount of tritium) into vacuum and have reached the downstream neon layer, after passing through the downstream protium layer. The shape of the peak is characteristic of the energy dependence of the $\mu t + H_2$ scattering cross section. The position of the maximum corresponds to the energy at the Ramsauer-Townsend minimum. As described in previous paragraphs, early time events (between 0 and 0.3 μs) are visible.

During the data-taking of 1996, we have noticed that we had the possibility to measure simultaneously

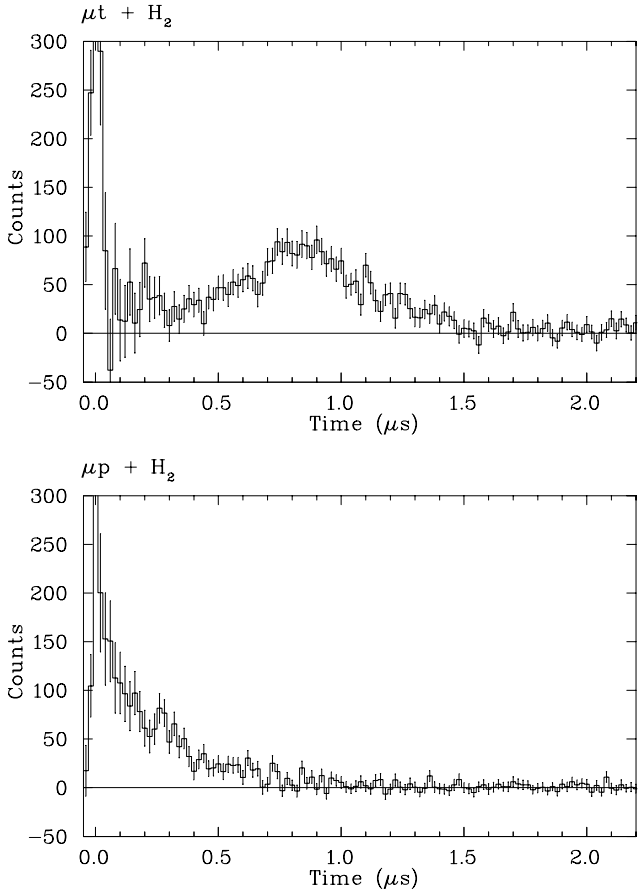

Fig. 60. Top: μNe x-ray time spectra produced after muon transfer from μt atoms to neon, with protium on top of the downstream neon layer. Bottom: μNe x-ray time spectra produced after muon transfer from μp atoms to neon, with neon on top of the upstream protium layer.

the time spectra and yields of γ-rays and conversion muons from the $pd\mu$ fusion reactions:

$$\begin{aligned} pd\mu \quad \rightarrow \quad & \mu^3\mathrm{He} + \gamma \;\; (E_\gamma = 5.5\,\mathrm{MeV}) \\ & {}^3\mathrm{He} + \mu_{\mathrm{conv}} \;\; (E_\mu = 5.3\,\mathrm{MeV}). \end{aligned}$$

By performing a series of measurements at different concentrations of deuterium, we obtained a confirmation of the Wolfenstein-Gershtein effect. This effect predicts an enhancement of γ's and μ's $pd\mu$-fusion yields at increased deuterium concentrations, due to the spin-flip transitions between the hyperfine levels of the muonic atom. Figure 61 shows a comparison between the experimental yield ratio and the theoretical predictions. The simultaneous measurement of both fusion products will give precise information about nuclear fusion rates in the different spin state populations of the $pd\mu$-molecules.

A similar effect should be observed in the $pt\mu$-fusion with the following reactions:

$$\begin{aligned} pt\mu \quad \rightarrow \quad & \mu^4\mathrm{He} + \gamma \;\; (E_\gamma = 19.8\,\mathrm{MeV}) \\ & {}^4\mathrm{He} + \mu_{\mathrm{conv}} \;\; (E_\mu = 19.2\,\mathrm{MeV}). \end{aligned}$$

In addition to the Wolfenstein-Gershtein effect, there is a discrepancy of more than two orders of magnitude between the theoretical relative fusion yield μ/γ and the only experimental result available to date. Unfortunately, due to beam problems, we did not succeed in performing the required measurements in 1997. On a test run of less than 5 hours, we succeeded in observing the 19.2 MeV μ simultaneously with the 19.8 MeV γ. The on-line analysis gave a ratio μ/γ which lies between the existing theoretical and experimental values. More beam time would be required to solve this interesting puzzle.

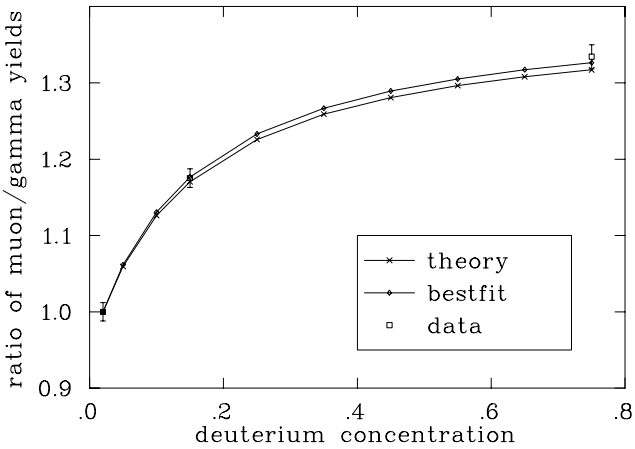

Fig. 61. The ratio of muon yield over gamma yield with respect to deuterium concentration.

Experiment 749
Muonium-substituted free radicals
(P.W. Percival, SFU)

The purpose of Expt. 749 is to study the structure and intramolecular motion of organic free radicals. Muon hyperfine constants are measured by transverse-field muon spin rotation (μSR) and, where necessary, radio frequency muon spin resonance (rf-μSR). Other hyperfine constants are determined by muon level-crossing resonance (μLCR). The temperature dependence of the hyperfine constants can be used to deduce the preferred molecular conformation and/or configuration, and the barrier to the internal motion, such as rotation about a carbon-carbon bond, or configuration inversion.

Several different radical systems have been studied in Expt. 749. Of current interest are the muonium adducts of fullerenes, pyrene and pyrenophane. They are related by the question: How does curvature of an unsaturated carbon skeleton affect radical adduct formation?

TRIUMF was the first laboratory to initiate μSR studies of buckminsterfullerene, C_{60}, and has been in the forefront of subsequent studies of C_{60}, C_{70}, and their derivatives. It is significant that HC_{60} was only detected (by electron spin resonance, at NRC Ottawa) when the hyperfine constant could be estimated on the basis of the MuC_{60} result. Experiment 749 and its predecessor Expt. 654 have concentrated on the structure and reactivity of fullerenes, in particular the distribution of the unpaired electron in the radical adduct, since that determines the reactivity of inequivalent sites.

The spin distribution in MuC_{60} was determined by applying μLCR to a dilute solution of $^{13}C_{60}$ [Percival *et al.*, Chem. Phys. Lett. **245**, 90 (1995)]. This work provided for the first time the signs of the hyperfine constants, which are required to resolve ambiguities in assignments when experimental data are compared with computed spin densities. This is even more important in the case of C_{70}, since there are five inequivalent groups of carbon atoms where Mu (or H) could add, each giving a unique radical. Of the five possible radicals three were first detected at PSI [Niedermayer *et al.*, Phys. Rev. **B47**, 10923 (1993)] and a fourth at TRIUMF [Addison-Jones *et al.*, Hyp. Int. **86**, 817 (1994)]. However, structural assignments are uncertain, and a claim to a fifth radical signal [Lappas *et al.*, J.C.S., Chem. Comm. **1994**, 2743 (1994)] is inconsistent with calculations [Borghi *et al.*, J. Am. Chem. Soc. **118**, 7608 (1996)].

It is generally accepted that the missing radical corresponds to Mu addition at site E (see Fig. 62). Unlike the other four sites, E is at the intersection of three six-membered carbon rings. The lack of a five-membered ring accounts for the reduced curvature of the C_{70} skeleton around the equator. In this respect, the equatorial region of C_{70} resembles a polycyclic aromatic hydrocarbon. A pyrene-like structure is marked in bold in Fig. 62.

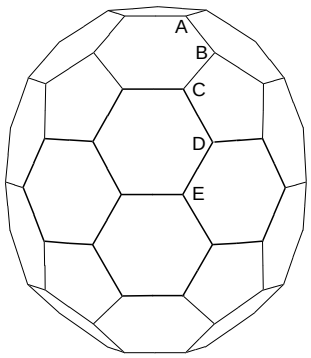

Fig. 62. Front face of the C_{70} molecule, showing examples of the five inequivalent carbon atoms (A to E) and a pyrene-like fragment (in bold).

As reported last year [1996 TRIUMF Annual Report, p. 55] it has been established that Mu mainly adds to positions 1 and 4 of pyrene (and symmetrical equivalents; see Fig. 63 for the numbering convention), with a small probability of 2. At these three sites Mu addition results in a tetrahedral -CHMu- configuration. There was no indication of Mu addition to the tertiary carbons (11 and 15). These sites are unreactive because of the rigidity of the planar carbon skeleton at the points of ring fusion. On the other hand, it is precisely such sites that are attacked in fullerenes, which have curved carbon structures.

Thus, to mimic a fullerene it is necessary to introduce curvature to the polyaromatic hydrocarbon. How can you do this? Tie the ends together! In effect this is what is done in the molecule 1,8-dioxa-[8](2,7)pyrenophane (Fig. 64). The angles between adjacent planes of carbon atoms average 15°, similar to parts of C_{70} and C_{84} [Bodwell *et al.*, Angew. Chem. Int. Ed. Engl. **35**, 1320 (1996)]. Most of the beam time used by Expt. 749 over the past year has been expended in

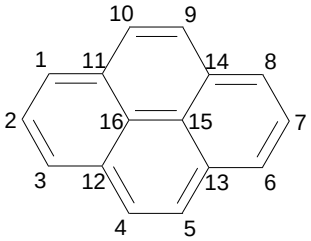

Fig. 63. Pyrene, an important polyaromatic hydrocarbon.

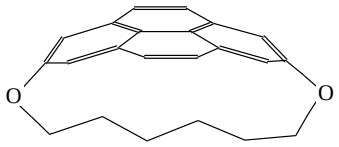

Fig. 64. 1,8-dioxa-[8](2,7)pyrenophane, a 'bent' pyrene.

the study of a solution of this pyrenophane in tetrahydrofuran.

The transverse field μSR spectrum revealed a pair of radicals with muon hyperfine constants 295.4 MHz and 391.0 MHz, about 12% larger than for 1-Mu-pyrenyl and 4-Mu-pyrenyl, respectively. Such an increase is qualitatively consistent with a less extensive distribution of unpaired spin in the pyrenophane. However, the μLCR spectrum is complex and can not be understood by simply scaling the pattern of resonances found for the pyrenyls. Comparison of experimental results with predictions based on density functional calculations suggests the inequivalence of *endo*- and *exo*-adducts to the edge carbons. Analysis of the results is incomplete, but the μSR and μLCR signals are tentatively assigned to the *exo*-1-Mu-(2,7)pyrenophane and *exo*-4-Mu-(2,7)pyrenophane.

Experiment 758
Electronic structure of muonium and muonium-lithium complexes in graphite and related compounds
(J. Chakhalian, R.F. Kiefl, UBC)

The purpose of this experiment is to explore the formation and electronic structure of muonium in graphite and related compounds. Muonium is the bound state between a positive muon and an electron which has been well studied in nonconductive materials such as insulators and intrinsic semiconductors. The unpaired electron on the muon produces large hyperfine interactions both on the muon and neighbouring nuclear spin which can be used to identify and characterize the local electronic structure of muonium in solids. In semiconductors studies of muonium are used to model the behaviour of atomic hydrogen which is itself very difficult to study in an isolated form. It is much more difficult to identify muonium in conductive materials where the unpaired electron spin is strongly coupled to the conduction electrons. In this case muonium is expected to act as a Kondo impurity, the study of which has intrigued physicists for more than 30 years. Recently we have discovered evidence for local moment formation on the muon in several metallic media with low carrier concentrations – such as alkali fullerides (Expt. 658), the semi metal antimony (Expt. 668), and n-type semiconductors (Expt. 752). The signature for muonium in metallic media is a large temperature dependent muon Knight shift and correspondingly large $1/T_1$ spin relaxation rate.

The focus of Expt. 758 is the semi metal graphite which is a particularly simple elemental compound. We are also studying the influence of Li intercalation on muonium. This is also interesting since graphite and related compounds are used in lithium batteries and recently it was observed that the capacity of these compounds to hold Li was proportional to the hydrogen content. One possibility is that a LiH complex is formed. Since the muonium mimics the behaviour of hydrogen we anticipate that the muon may form a similar complex in Li intercalated graphite.

In order to make a precision muon Knight shift measurement in graphite we have developed a specialized μSR apparatus to collect data on a sample and a reference simultaneously. This allows us to measure the precision frequency shifts relative to a reference under identical experimental conditions. This year we have made significant improvements to the apparatus. In particular we have replaced a plastic light guide in the cryostat with a hollow reflective guide using silverized mylar. This removes previous systematic problems below 30 K which were traced to the Curie-like magnetic susceptibility of plastic. In addition for the studies above room temperature we have made it possible to collect a reference spectrum whereas before this was not possible in the oven. The typical statistical accuracy on individual frequencies is currently about 2 ppm after an hour of data collection (10^7 events) whereas the systematic error on the frequency shift is at about the same level.

Figure 65 shows the temperature dependence of the Knight shift measured with the magnetic field parallel and perpendicular to the $\vec{c}$ axis of HOPG graphite. Figure 66 shows the isotropic and axial parts of the Knight shift. Both the magnitude of the Knight shift and its large temperature dependence are evidence for local moment formation. For example the ratio of the Knight shift relative to the electronic spin susceptibility is extremely large – about 700 times greater than that observed in free electron-like metals such as silver.

The observed temperature dependence of the Knight shift can be explained qualitatively using the following two state model. We assume that there are two possible electronic states for muons – one which is paramagnetic with a single unpaired electron (e.g. neutral muonium) and the other which is a spin singlet in which the conduction electrons effectively screen the local electronic moment of muonium. In order to explain our results the binding energy for this screening cloud must be on the order of 700 K. One could imagine the singlet state to be the negative charge state of muonium with two bound electrons although the

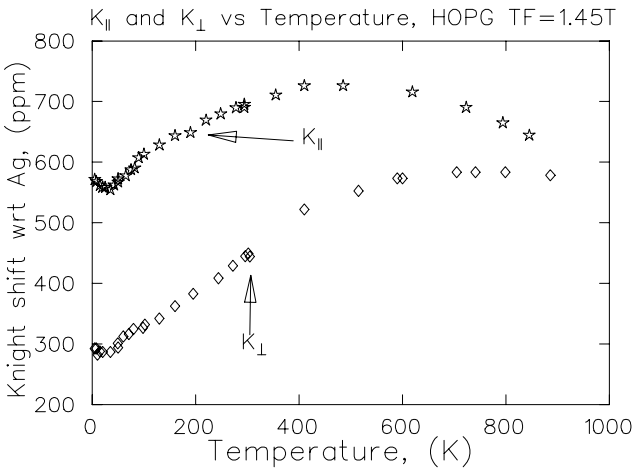

Fig. 65. The muon Knight shift parallel to the c axis in HOPG graphite versus temperature. Below room temperature (RT) the data were taken in the cryostat whereas the oven was used above RT.

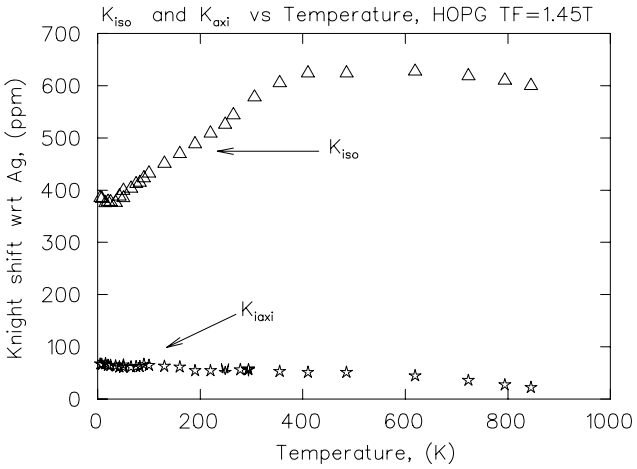

Fig. 66. Temperature dependence of isotropic $K_{\rm iso}$ and axial or dipolar $K_{\rm axi}$ parts of the Knight shift in HOPG graphite.

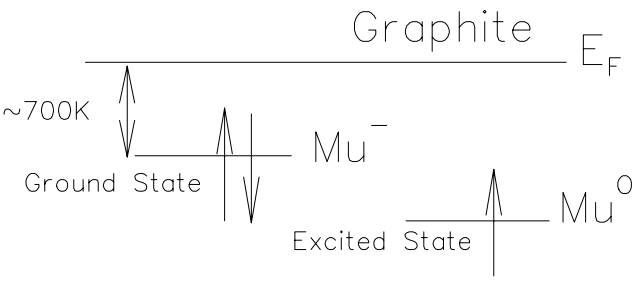

Fig. 67. Schematic illustration of the proposed phenomenological model. Details are given in the main text.

actual electronic structure of the sreened state is likely to be much more complicated since it would be strongly hybridized with the conduction electrons. Figure 67 illustrates the position of the proposed two states with respect to the fermi level. At the lowest temperature one observes a Knight shift characteristic of the spin singlet ground state. As in the case of Kondo impurities the local spin susceptibility is, however, still large due to mixing in of the low lying excited states involving the neutral paramagnetic muonium. As the temperature is raised the Knight rises due to the thermal occupation of the paramagnetic excited state. In other words the electrons which screen the magnetic moment are shaken off. Above 600 K the Knight shift turns over and starts to decrease. This is also expected since once the electronic moment on the muon is fully exposed the 1/T Curie term characteristic of the paramagnetic muonium state eventually dominates.

Experiment 774
Muonium dynamics in GaAs
(S.R. Kreitzman, B. Hitti, TRIUMF)

The contribution of μSR research to the understanding of the behaviour of isolated hydrogen in semiconductors has been widely recognized. Our work in Si has produced a good understanding of the muonium charge state dynamics in this prototypic semiconductor. Experiment 774 is a long term research project to investigate muonium dynamics by radio frequency (rf) and (micro-) μ-wave μSR in the technologically very important compound semiconductor GaAs. This experiment received its first beam allocation in 1997, which was used to study the temperature dependence of the diamagnetic fraction in two commercial semi-insulating (SI) samples between 10 K and 600 K.

For comparison we display in Fig. 68a the temperature dependence of the diamagnetic amplitude in a well compensated slightly p-type Si sample. At low temperature approximately equal fractions of Mu^0_{BC} and Mu^0_T are present and the ionized fraction is essentially zero. As the temperature is increased the first observed transition is indicated by the sharp increase in the amplitude near 140 K. This corresponds to the ionization of Mu^0_{BC} to Mu^+_{BC}, whereby an electron is thermally promoted to the conduction band. This process was first assigned based on the disappearance of the Mu^0_{BC} signal at the same temperature in transverse field (TF) μSR. The second process to become active with increasing temperature is the ionization of Mu^0_T which shows up as a gradual increase in the amplitude of the diamagnetic signal centered near 270 K, approximately where Mu^0_T is known to ionize from TF data. Above room temperature, cyclic electron capture and ionization results in the loss of the muon polarization and the sharp drop observed near 400 K. By studying ten n- and p-type Si samples of varying concentrations, we developed a model of muonium dynamics, extracted energy levels within the bandgap for the neutral centres and determined the parameters (prefactor rates, barrier and cross sections) which govern interconversions between the muonium centres.

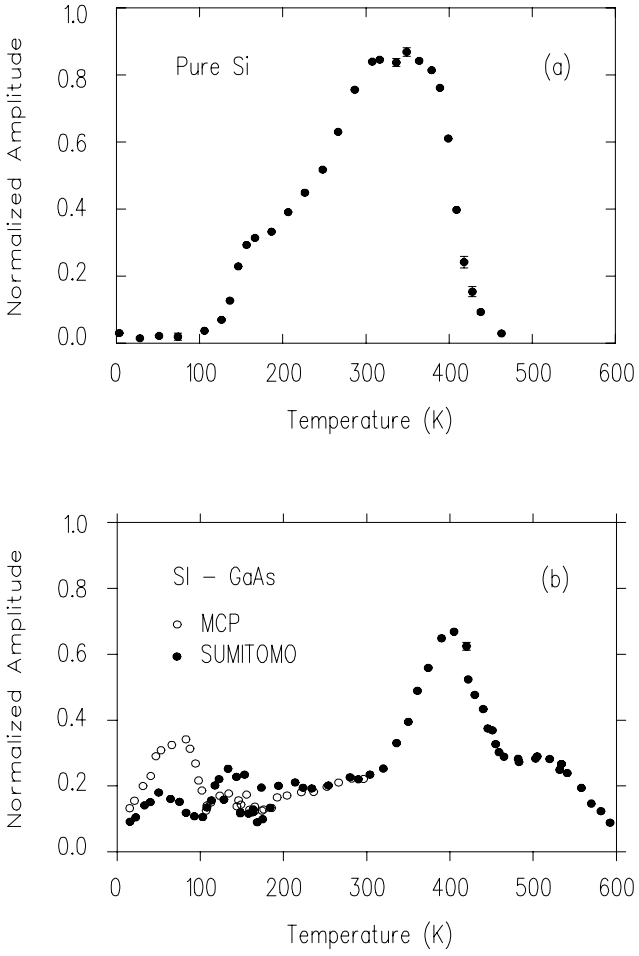

Fig. 68. The temperature dependence of the diamagnetic fraction measured by radio frequency μSR near 2 kG in high resistivity Si (a) and two commercial semi-insulating GaAs (b) samples.

The temperature dependence of the diamagnetic fraction measured at 2 kG in two intrinsic high resistivity GaAs samples between 10 K and 600 K is displayed in Fig. 68b. The Sumitomo material had no previous exposure to a beam prior to the taking of this data whereas the MCP sample was measured at ISIS before the runs at TRIUMF. Several differences are apparent in the behaviour of the diamagnetic amplitude as a function of temperature in Si (Fig. 68a) and GaAs (Fig. 68b).

As the temperature is increased the first feature observed in GaAs is the peak near 50 K. Both GaAs samples show this feature, however, the peak in the MCP sample is more prominent. While an increase in the diamagnetic amplitude below 50 K was observed in some of the Si samples (not displayed) and shown to result from the ionization of shallow dopant, no drop was seen at low temperature in any of the Si samples studied.

Between 100 and 200 K, the Sumitomo sample shows "scatter" in the data. The data falling on the *high branch* were taken during the first portion of the run, whereas the *lower branch* was measured during the final phases of the run. Although checks were made, the cause for this discrepancy is not yet known. The other data points were all accumulated in a somewhat random fashion throughout the course of the run and did not show any erratic behaviour.

Based on TF data, Mu^0_{BC} and Mu^0_T in both Si and GaAs are expected to ionize below room temperature. In Si the diamagnetic amplitude measured by rf increases sharply near 140 K, the ionization temperature of Mu^0_{BC} and gradually near 270 K, the temperature at which Mu^0_T is expected to ionize. In both GaAs samples the diamagnetic fraction did not increase at the expected ionization temperatures of the neutral muonium states. In fact, the amplitude in GaAs remains low at about 20% up to room temperature and then increases and peaks near 400 K.

Finally, the sharp drop observed in Si above room temperature was shown to be the result of charge exchange involving conduction band electrons. In GaAs at high temperature there is a drop in the amplitude that starts just above 400 K followed by a plateau centered around 500 K and then a second drop. Since the bandgap in GaAs is wider than in Si only the drop centered around 550 K is expected to result from charge exchange involving electrons thermally ionized across the bandgap.

As observed from the results summarized in this report the problem of analyzing the dynamics of muonium in GaAs is very different from that in Si. The presence of intrinsic defects related to deviations from ideal stoichiometry and structure makes it difficult to obtain sample independent data on SI GaAs. In this respect during the next available beam time we plan to investigate high quality LPE (liquid phase epitaxy) samples with the level of intrinsic impurities into the 10^{13} cm^{-3} range. These samples should provide the data needed to clarify the mechanisms of muonium dynamics in GaAs.

Experiment 775
Electron transport in insulators, semiconductors and magnetic materials
(J.H. Brewer, UBC; G.M. Luke, Columbia; V. Storchak, Kurchatov Inst.)

The primary goal of Expt. 775 is to better understand electron transport in insulators and semiconductors (e.g. the transition between coherent propagation of bandlike states and the incoherent hopping of localized states) using as an experimental tool the phenomenon of delayed muonium (Mu) formation (DMF) via transport to the thermalized muon of the excess electrons liberated in the muon's ionization track.

DMF can be inhibited by applying an external electric field to the sample in which the muons stop, overcoming the Coulomb attraction of the μ^+ for the nearest free e^-.

This method has been developed under Expt. 693 (see previous Annual Reports) for the special insulators known as cryocrystals (solids composed of atoms or molecules which are gaseous at room temperature and atmospheric pressure) such as the rare gas solids and certain molecular solids like solid nitrogen (s-N_2).

Under Expt. 775 these measurments are being extended to "ordinary" nonmetals including technologically important semiconductors (Si, Ge, GaAs, etc.) and insulators (SiO_2, Bi_2O_3, etc.) as well as more complex materials such as the base compounds for high temperature superconductors and exotic magnetic insulators where other manifestations of highly correlated electrons are currently under intense study. In the latter cases our motive is to determine whether the muon itself or its radiolysis products may be affecting magnetic interactions in such a way as to mask the effects being investigated by μSR.

Cryocrystals

Note the large difference (Fig. 69) between liquid and solid Ne in contrast with a smaller and opposite difference between liquid and solid Ar. In each case an electric field in the positive direction (along the original direction of motion of the incoming muon) is more effective at reducing DMF than a negative E, indicating that the muon generally stops downstream of the location of its last radiolysis electron – and that the general direction of motion of the muon is preserved down to energies of ∼10–100 eV. However, in the rare gas solids the anisotropy is much weaker than in the molecular solids or in liquid neon.

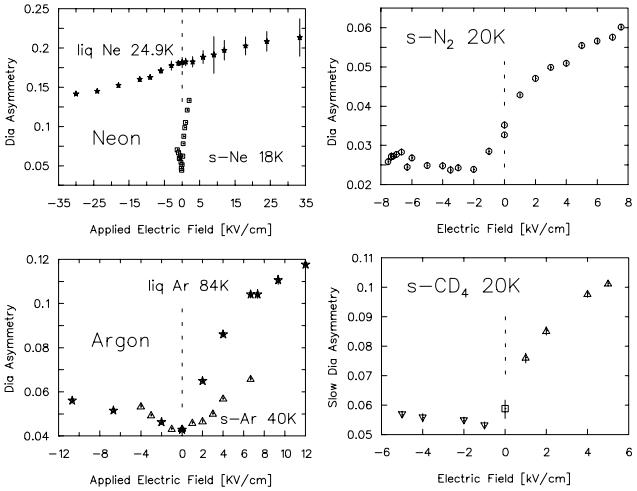

Fig. 69. Comparison of the electric field dependence of the diamagnetic asymmetry A_D in selected cryocrystals and cryoliquids. The muonium (Mu) asymmetry is roughly half the difference between A_D and the full asymmetry $A_0 \approx 0.2$ in each case. That is, whenever A_D is less than about 0.2, it is due to Mu formation; an increase in A_D reflects inhibition of Mu formation.

"Ordinary" nonmetals

Note that in GaAs one can almost completely eliminate muonium formation by applying a large electric field, whereas the electric field has only a modest effect on mounium formation in silicon (Fig. 70). The horizontal scale also varies widely, due to limitations imposed by electrical breakdown in the materials (or the apparatus).

Very slow Mu formation

In the spinless rare gas solids like s-Ne and s-Ar, it is especially obvious that, in addition to the DMF process leading to a coherent Mu precession signal, there is a very slow DMF process causing "relaxation" of the diamagnetic signal on a timescale of microseconds. This decay is affected by an applied electric field in just the same way as the fast DMF, indicating that the electrons involved have roughly the same spatial distribution about the stopped μ^+ but have a lower mobility by as much as 5 orders of magnitude. These electrons are self-trapped by polarizing and/or repelling the surrounding atoms; the resultant polarons may be thought of as quasiparticles (renormalized electrons, in particle physics language) whose effective masses are much larger than the free electron mass.

This phenomenon is of interest for at least two reasons: first, slow DMF is the main cause of rapid muon relaxation in sapphire and is strongly temperature dependent; this may have a confounding effect on certain

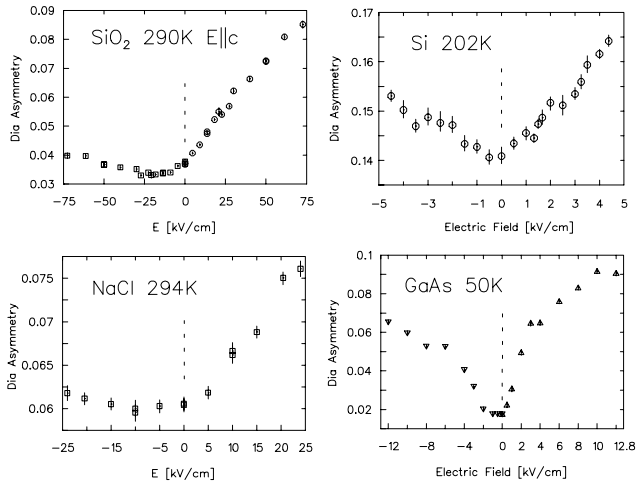

Fig. 70. Comparison of the electric field dependence of the diamagnetic asymmetry A_D in selected "ordinary" semiconductors and insulators. Although the mean separation of the muon from its last radiolysis electron is generally smaller than in cryocrystals, requiring a larger electric field to inhibit DMF, the qualitative phenomenology is the same.

delicate measurements of muon relaxation in longitudinal fields. Second, the identification of (at least) two separate species of negative charge carriers created by ionization in liquid and solid argon may have important implications for the design of particle detectors such as the large ℓ-Ar calorimeter in the ATLAS experiment (see Table II).

Table II. Rough estimates of mean distance $\langle R_{e\mu}\rangle$ between the μ^+ and its last radiolysis electron after both have just thermalized in different condensed media.

Medium	T [K]	$\langle R_{e\mu}\rangle$ [nm]
liquid neon	24.9	20
solid neon	18	80
liquid argon	84	50
solid argon	40	35
solid α-N_2	20	50
solid CD_4	20	60
SiO_2 (quartz)	290	15
NaCl	294	20
silicon	202	40
GaAs	50	60

The distance $\langle R_{e\mu}\rangle$ is estimated by equating the electric field $E_\mu = e/\epsilon\langle R_{e-\mu}\rangle^2$ of the muon at that distance with the external electric field required to inhibit delayed muonium formation by about half.

Experiment 776
Rare earth materials with disordered spin structures
(D.R. Noakes, Virginia State)

This experiment uses muon spin relaxation (μSR) to study the local magnetic fields in rare earth quasicrystals (icosahedral (*i*-)RE-Mg-Zn, RE=rare earth) and crystalline induced-moment spin glasses PrP_x. It was motivated by Expt. 665 (transition-metal quasicrystals) and Expt. 640 (low-carrier-density Kondo-lattice CeNiSn and related materials), where we observed similarly anomalous zero-field (ZF) muon spin relaxation functions in *i*-Al-Mn-Si and Ce(Ni,Cu)Sn alloys. The anomalous feature was static muon spin relaxation below the spin glass temperatures, T_g, with polarization-minima too shallow to be consistent with any of the field distributions previously identified in solids (in some cases the minima were *non-existent*). It was natural to extend such measurements to rare earth quasicrystals once samples became available, and because it was suggested that the shallow minima might be a consequence of "induced-moment" spin glass behaviour, where only ions adjacent to the right kind of impurity or defect have magnetic moments, we decided to measure the archetype of that behaviour, PrP_x.

Quasicrystals tend to form only for narrow ranges of composition of their elements. The *i*-Al-Mn-Si samples of Expt. 665 had compositions $Al_{75.5}Mn_{20.5}Si_4$ and $Al_{73}Mn_{21}Si_6$, yet above the spin-glass freezing temperature, T_g, these samples generated μSR spectra consistent with those from dilute-moment spin glasses. In particular, there was no coupling of any electronic magnetic moments to the muons at temperatures above 2 T_g. This suggests no more than three magnetic ions per hundred in these samples, and hence that only a fraction of the manganese ions possess magnetic moments. For Expt. 776, our samples had compositions $Gd_8Mg_{42}Zn_{50}$ and $Tb_8Mg_{42}Zn_{50}$, each with only eight magnetic ions per hundred, yet above T_g, these generated μSR spectra more consistent with dense-moment disordered magnetism. There was temperature dependent relaxation indicating coupling of the moments to the muons up to at least 200 K, and the relaxation rate increased dramatically (seemingly divergent) as temperature was lowered toward T_g. There were interesting differences between the two samples, however. The relaxation rate for the terbium sample was much larger than for the gadolinium sample, which we believe is due to "crystalline electric field" (CEF) splitting of the magnetic substates of the terbium f electrons, inducing single-ion anisotropy and reducing the ion fluctuation rate, thereby increasing the effective coupling to the muon (gadolinium remains isotropic). More strangely, however, while the Gd sample ZF-μSR was monotonic exponential, the Tb sample relaxation was monotonic but not exponential. It could be phenomenologically as "power-exponential" relaxation:

$$G_z(t) = A_0 \exp\left(-[rt]^p\right),$$

where the power decreased from near unity (ordinary exponential) at 200 K to 0.5 at 40 K (still far above T_g =12 K). Below that, the initial relaxation was so fast it could no longer be properly resolved: it was "lost in the initial dead time" of the apparatus. This sort of power-exponential relaxation in some disordered magnetic systems is an outstanding problem in μSR. In this case it can apparently be turned on and off by changing the magnetic ion anisotropy, but we do not understand why.

Below T_g in dilute spin glasses, it is often possible to continue to resolve ZF-μSR, and this was true of *i*-Al-Mn-Si in Expt. 665. The observed relaxation function, however, was of an unexpected and difficult to explain form: static monotonic relaxation to the 1/3-asymptote (as described in Noakes *et al.* [Phys. Lett. **A199**, 107 (1995)]). Similar relaxation functions were subsequently observed in ZF-μSR of Ce(Ni,Cu)Sn Kondo-lattice materials in Expt. 640, and Noakes and Kalvius [Phys. Rev. **B56**, 2352 (1997)] discovered an analytic form that fit the data: the static

"Gaussian-broadened Gaussian" Kubo-Toyabe relaxation function (described in our previous Annual Report). This indicates the form of local field distribution that must be operating, but not what configuration of moments in a material might generate such a field distribution. We speculated in the Phys. Lett. above that "range-correlated moment-magnitude variation" (RCMMV) was involved. Work on this idea is continuing with Monte Carlo simulation of RCMMV among ion moments in a material. While the implementation is still somewhat crude at this time, it indicates that RCMMV can produce the phenomenon of arbitrarily-shallow static ZF relaxation, and is beginning to indicate the association between the correlation range and the depth of the Kubo-Toyabe polarization minimum.

As temperature is lowered toward the magnetic freezing (or ordering) temperature of a concentrated magnetic system, on the other hand, the local fields are so large that ZF muon relaxation will often become too rapid to be resolved with standard μSR apparatus. This was already mentioned for *i*-Tb-Mg-Zn below 40 K. The reduced-asymmetry signal then seen has been difficult to interpret in whatever material it occurs in: at best it reflects only the fluctuation rate of the most-strongly frozen spins (and they may be a minority of the total). In our experiments, the *i*-Gd-Mg-Zn signal, being more slowly relaxing than for the Tb sample, could be followed down to and through $T_g \sim$ 7 K, indicating a complex inhomogeneous-freezing process, but the relaxation eventually became too rapid below 3 K, while still clearly dynamic (spins were not yet fully frozen). The M15 dilution refrigerator allowed us to reach much colder temperatures, likely to provide access to the static limit, where the field distribution can be seen more directly without the complication of field fluctuations, but ZF-μSR spectra by themselves were uninformative, since most of the signal was lost in the dead time. Using the superconducting magnet in the dilution refrigerator, we also took longitudinal field (LF) μSR spectra, which partially decoupled the muons from the static local fields which were essentially static at these low temperatures. This slowed the relaxation enough that it was detectable again for LF in excess of 1 Tesla. To our knowledge this is the first time that LF has been used to bring relaxation back from the dead time. It showed that the local field distribution is similar in shape (consistent with Gaussian) and in *rms* field in the frozen state of the two rare earth quasicrystals.

European workers, making their own *i*-RE-Mg-Zn samples, have reported [Charrier and Schmitt, Phys. Rev. Lett. **78**, 4637 (1997)] neutron diffraction indicating magnetic quasi-lattice ordering at ∼20 K in these materials, but could find no corresponding signal in bulk magnetization [J. Magn. & Magn. Mater. **171**, 106 (1997)]. Our μSR spectra show no evidence of any transition in the spin system near 20 K, making it difficult to believe there is any substantial bulk ordering occurring. Our rare earth quasicrystal μSR work is described in a paper to be published in Phys. Lett. A.

Meanwhile, our μSR spectra of the prototypical induced-moment spin glass PrP_x are unlike any of those from any of our quasicrystals, and also unlike the Ce(Ni,Cu)Sn spectra of Expt. 640. We have so far seen no spin glass freezing: instead ZF and low-LF μSR spectra appear to be consistent with "pure" dynamic Lorentzian Kubo-Toyabe relaxation. By "pure", we mean that we do not see the locally-Gaussian dynamics in a globally-Lorentzian field distribution that Uemura showed applied for dilute spin glasses, but rather that the local field fluctuations sample the complete Lorentzian field distribution for each and every muon stopped. While this might be due to muon hopping, that seems unlikely for such a complicated, and defected, crystal structure. We are trying to develop an explanation based on fluctuations of the praseodymium among CEF-split *f* substates, from non-magnetic ground to magnetic excited states. The temperature dependence of the local field fluctuation rate deduced from dynamic Lorentzian fits to the μSR data indicate an activation energy comparable to the energy reported for the first excited CEF state (∼ 48 K).

Experiment 777
Transverse field μ^+SR in $NbSe_2$

(R. Miller, UBC)

Motivation

Experiment 777 was proposed to investigate the vortex state of conventional superconductors with μ^+SR. Despite the popularity of research into high temperature superconductors, recent theoretical and experimental work has also focused on conventional superconductors. In particular, theoretical calculations have shown that the behaviour of conventional superconductors is still not very well understood, particularly at low temperatures.

Current understanding of vortex cores in *s*-wave superconductors

Many recent articles about conventional superconductors followed the 1989 discovery with scanning tunneling microscopy (STM) of bound states in the vortex cores of $NbSe_2$. These bound states were predicted theoretically in the 1960's, and shown in 1974 by Kramer and Pesch to give rise to a sharp shrinking in the vortex core with decreasing temperature. Recent numerical calculations have confirmed their prediction.

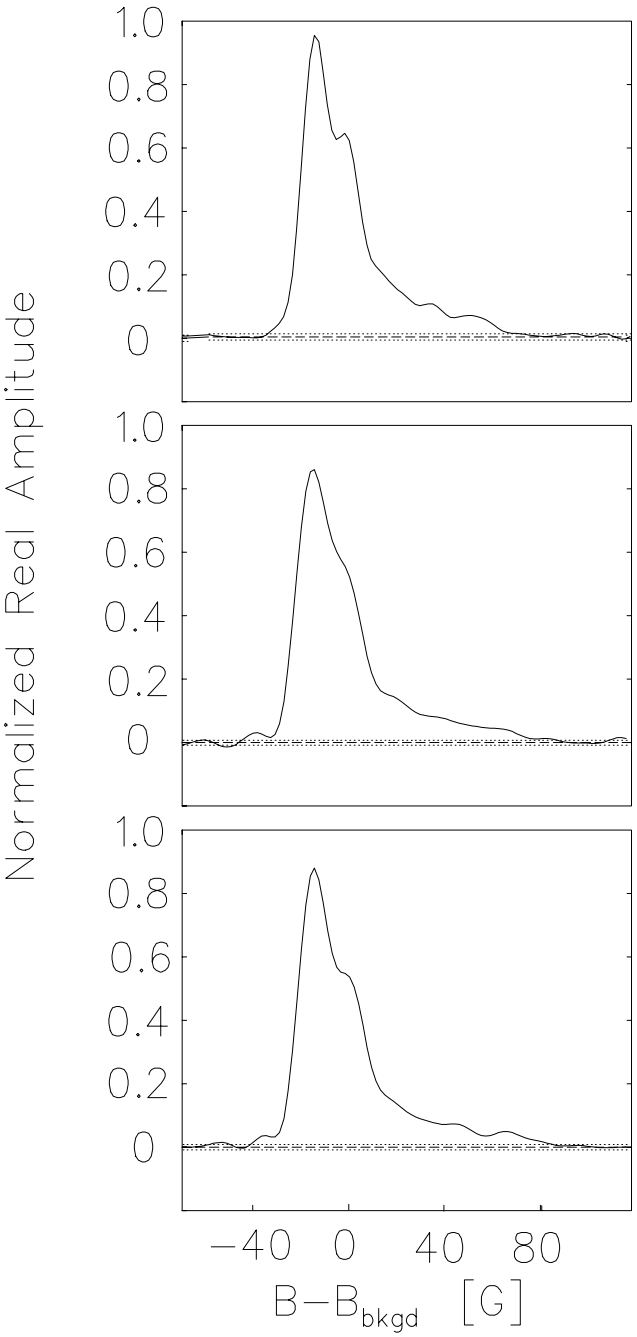

Fig. 71. Fourier transforms of the muon spin polarization. Top pane, $T = 2.4$ K; middle, $T = 0.5$ K; bottom, $T = 50$ mK. Data taken on M15 in a 5 kG field. Notice the high field tail due to the vortex cores.

The nature of the bound states is still somewhat uncertain, as well as their contributions to the supercurrent. However, these predictions are in strong disagreement with the popular Ginzburg-Landau theory, which predicts a constant core radius at low temperature.

$NbSe_2$ sample

Recent work on conventional superconductors has focused on $NbSe_2$. This material is also well suited for μSR since the geometry of the vortex lattice is well known to be triangular and the magnitude of the upper critical field, H_{c_2} is much smaller than that of high-T_c materials. The small value of H_{c2} provides an ideal situation for the study of the vortex core region in a magnetic field range most appropriate for a μ^+SR experiment. The cores then occupy a sizeable fraction of the sample so that the structure of the cores can influence the measured field distribution.

It has also been established through STM and small angle neutron scattering measurements that the vortex lattice is nearly perfect and free of pinning impurities. Our measurements confirm that pinning of the lattice is negligible.

Temperature dependence of the core radius in $NbSe_2$

Figure 71 shows the field distribution in $NbSe_2$ as measured by μ^+SR. Notice the high field tail due to the vortex cores. The cutoff is a measure of the vortex core radius.

Figure 72 shows the behaviour of the core radius as the temperature is varied from 50 mK to 4 K in an applied field of 5 kG. The core radius was defined as the distance from the core centre to the maximum in the supercurrent density. Note that there are four separate sets of data, each confirming the linear dependence

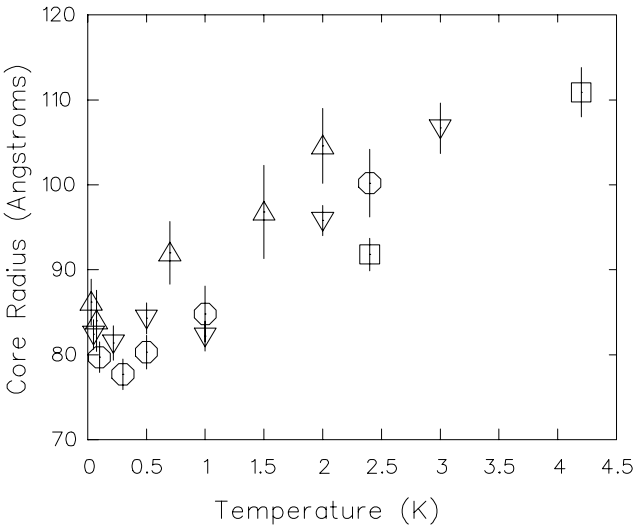

Fig. 72. The temperature dependence of the vortex core radius in $NbSe_2$ at 5 kG. Squares are data taken on M20; circles, July M15; triangles, November M15; inverted triangles, December M15. Measurements on M20 were taken in the Helios cryostat while measurements on M15 were taken in the dilution refrigerator. Notice that all the data suggest a linear temperature dependence in the core radius.

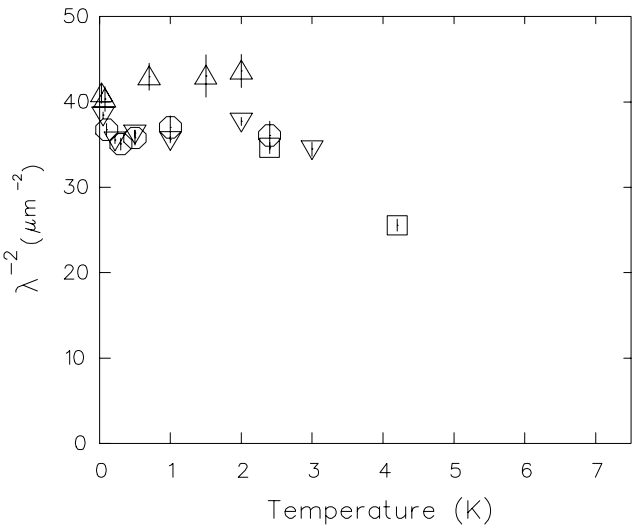

Fig. 73. The temperature dependence of λ_{ab}^{-2} (T) in $NbSe_2$ at 5 kG. See caption of Fig. 72 for symbols. Notice that the penetration depth is constant at low temperature. T_c= 7.0 K.

of the core radius with temperature. The different intercepts likely arise from systematic errors associated with different beam lines and set-ups.

The temperature dependence of the core radius is much weaker than theoretical predictions. A possible explanation for this disagreement is that all of the calculations were done in the single vortex approximation. Our previous work on $NbSe_2$ [Sonier *et al.*, Phys. Rev. Lett. **79**, 1742 (1997)] showed that the core radius is strongly field dependent, especially at low fields.

Figure 73 shows the dependence of the penetration depth on temperature in a 5 kG field. For each of the runs, the penetration depth is independent of temperature at low temperatures, as would be expected for an *s*-wave superconductor.

Conclusions

Our μ^+SR data on the temperature dependence of the vortex core radius confirm recent calculations based on microscopic theories, but disagree with the magnitude of the effect. This shrinking of the cores is due to the bound states in the cores as they become depopulated at low temperatures. Recent work suggests that the core radius should remain constant below a temperature on the order of the energy minigap between bound states.

Experiment 782
Non-fermi-liquid behaviour and other novel phenomena in heavy-fermion alloys

(D.E. MacLaughlin, California-Riverside)

Thermodynamic and transport measurements in certain heavy-fermion alloys indicate that the fermi-liquid description appropriate to a conventional spin-singlet Kondo system does not apply to these materials. Perhaps the most striking non-fermi-liquid (NFL) low-temperature anomalies are a linear temperature dependence of the resistivity and a logarithmic divergence of the Sommerfeld electronic specific heat coefficient. Both of these properties indicate a serious breakdown of the fermi-liquid picture, and both characterize nearly every NFL heavy-fermion system discovered to date.

Evidence has emerged from our μSR and NMR experiments [Bernal *et al.*, Phys. Rev. Lett. **75**, 2023 (1995); Bernal *et al.*, Phys. Rev. **B54**, 13,000 (1996); MacLaughlin *et al.*, J. Phys.: Condens. Matter **8**, 9855 (1996)] that in some cases this NFL behaviour is due to an inhomogeneous distribution of Kondo temperatures T_K arising from disorder in the random alloy. Such "Kondo disorder" implies a broad distribution of the heavy-fermion spin polarization, direct signatures of which are correspondingly broad μSR and NMR lines at low temperatures. The goals of our μSR studies of NFL behaviour are (a) to ascertain the applicability of the Kondo disorder mechanism to a number of NFL materials, and (b) to determine whether static magnetism, which could affect bulk properties and masquerade as NFL behaviour, is present.

We have obtained preliminary results for three "Kondo hole" NFL systems ($La_{0.8}Ce_{0.2}Cu_{2.2}Si_2$, $Th_{0.94}U_{0.06}Ru_2Si_2$, and $Th_{0.7}U_{0.3}Pd_2Al_3$) in which the f sublattice is diluted, and on the ligand-disorder alloy $CeRhRuSi_2$. Zero-field (ZF) μSR experiments were carried out on all of these systems to search for static magnetism (presumably spin-glass freezing). In addition, transverse-field (TF) μSR spectra in some samples were examined for the anomalous line broadening which is the principal signature of Kondo disorder [*op. cit.*].

ZF-μSR: no static magnetism

Figure 74 shows preliminary results for the temperature dependence of the ZF-μSR Kubo-Toyabe (K-T) relaxation rate Δ in $La_{0.8}Ce_{0.2}Cu_{2.2}Si_2$, $Th_{0.94}U_{0.06}Ru_2Si_2$, and $Th_{0.7}U_{0.3}Pd_2Al_3$. The K-T fits are good, and the rates are all slow and depend very little on temperature down to $\sim$2 K. Similar ZF-μSR behaviour was found in $CeRhRuSi_2$. This is evidence the relaxation is due to nuclear dipolar fields, and that there is no significant static magnetism, ordered or disordered, at low temperatures. Static magnetism, if present, could produce deviations of thermodynamic and transport properties from fermi-liquid behaviour and thus mimic NFL phenomena.

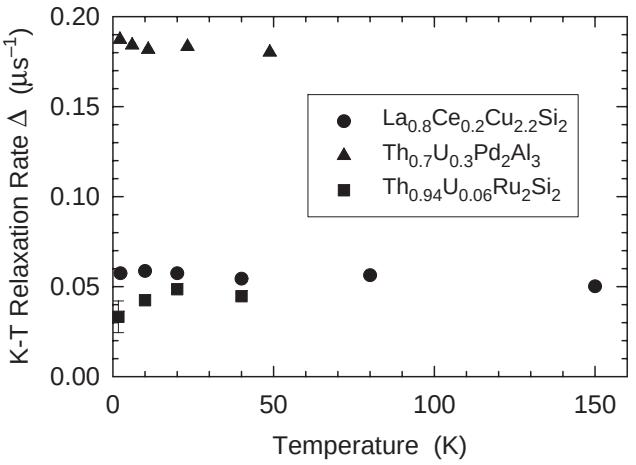

Fig. 74. Temperature dependence of μ^+ ZF Kubo-Toyabe (K-T) relaxation rate Δ in three non-fermi-liquid heavy-fermion alloys (preliminary data). The low values and slight temperature dependence are evidence for the absence of static magnetism down to $\sim$2 K.

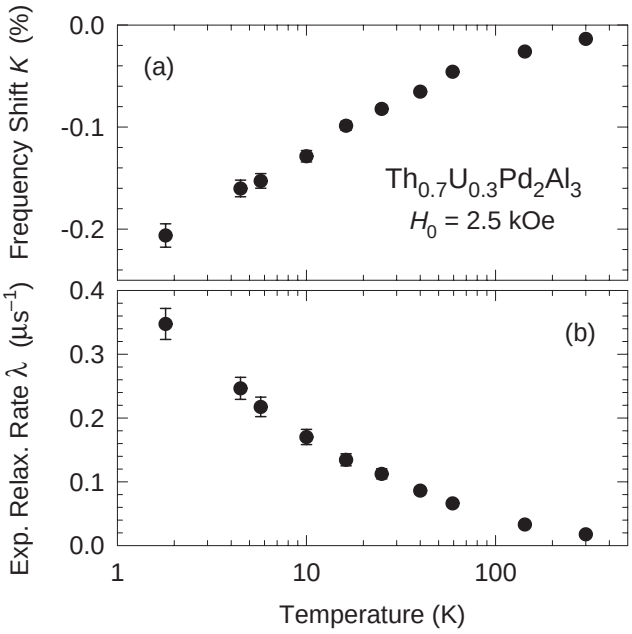

Fig. 75. Temperature dependence of TF-μSR spectral parameters in $Th_{0.7}U_{0.3}Pd_2Al_3$ obtained from "damped Gaussian" fits to the data. The Gaussian rate was fixed at $0.127\,\mu s^{-1}$. (a) Frequency shift K. (b) Exponential relaxation rate λ.

TF-μSR in $Th_{0.7}U_{0.3}Pd_2Al_3$

In $Th_{0.7}U_{0.3}Pd_2Al_3$ the shape of the TF relaxation function was found to change markedly with temperature: preliminary fits to a "power exponential"[1] $G(t) = \exp[-(Dt)^a]$ yielded values of a varying from $\sim$2 at 300 K to $\sim$1 at low temperatures. This behaviour can be understood as a crossover from nuclear dipolar broadening at high temperatures to relaxation at low temperatures by a Lorentzian[2] distribution of frequency shifts induced by the f-ion paramagnetism.

The TF relaxation functions were therefore fit to the "damped Gaussian" functional form

$$G_{\rm TF}(t) = \exp(-\tfrac{1}{2}\sigma_{\rm nuc}^2 t^2)\exp(-\lambda t)\,,$$

where the Gaussian factor accounts for the nuclear broadening and the exponential factor accounts for the paramagnetic broadening. This form is obtained when the spectrum is the convolution of (Gaussian) nuclear broadening with the (Lorentzian) distribution of paramagnetic frequency shifts. It should be noted that the exponential factor represents the effect of a *static* distribution of paramagnetic frequency shifts rather than dynamic lifetime broadening, which is ruled out by the observed slow Gaussian ZF-μSR relaxation.

The nuclear relaxation rate $\sigma_{\rm nuc}$ was estimated from the observed zero-field nuclear Kubo-Toyabe rate $\Delta_{\rm nuc}$ assuming strong quadrupolar splitting of the ^{27}Al nuclei responsible for the broadening; in this case $\sigma_{\rm nuc} = \Delta_{\rm nuc}/\sqrt{2} = 0.127\,\mu s^{-1}$. Frequency shifts K and exponential relaxation rates λ obtained in this manner for a transverse field $H_0 = 2.5$ kOe are shown in Fig. 75. Here $K = \nu/\nu_0 - 1$, where ν is the mean muon precession frequency and $\nu_0 = \gamma_\mu H_0/2\pi$ (γ_μ is the muonic gyromagnetic ratio) is the reference frequency in the applied field H_0. Both K and λ vary with temperature in a Curie-Weiss-like fashion, as expected in a paramagnetic alloy where the linewidth is due to an inhomogeneous distribution of shifts.

The important question is whether the behaviour of the linewidth is indicative of Kondo disorder, the primary signature of which is a large magnetic resonance linewidth due to a spread δK of shifts K. In the Kondo disorder model this linewidth is directly proportional to the corresponding spread $\delta\chi$ of the susceptibility χ ($\delta K/K = \delta\chi/\chi$ to within a factor of order unity), and varies substantially with temperature [*op. cit.*]. In f-sublattice-diluted alloys another contribution to the linewidth comes from the statistically distributed sites of the f ions, even if their polarization were uniform. In this case the linewidth, like the shift, tracks the magnetic susceptibility, so that the linewidth divided by the shift is constant.

From fits to our TF-μSR data we obtain δK from the relaxation rate λ: $\delta K = \lambda/2\pi\nu_0$. Figure 76 is a "Kondo disorder plot" of the fractional spread $|\delta K/K|$ vs. $|K|$ (for comparison with previous results from systems with Kondo disorder

[1] In this and the following the $G(t)$ are envelope relaxation functions from which the muon precession frequency has been removed.
[2] The line shape corresponding to exponential relaxation is Lorentzian, with linewidth $\Delta\nu$ related to the relaxation rate λ by $\Delta\nu = \lambda/2\pi$.

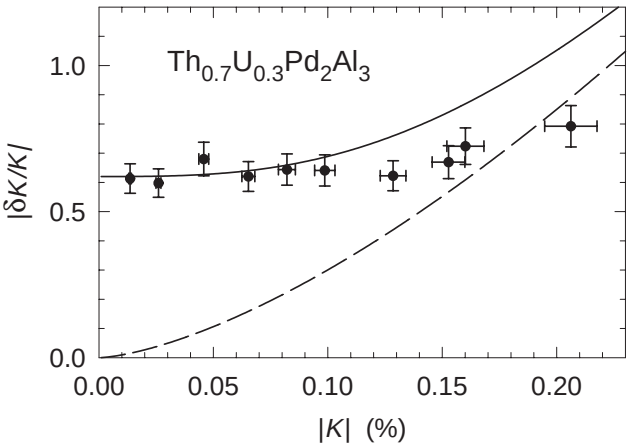

Fig. 76. "Kondo disorder plot" (relative μ^+ linewidth $|\delta K/K|$ vs. absolute frequency shift $|K|$) for the μ^+ shift and linewidth in $Th_{0.7}U_{0.3}Pd_2Al_3$. Points obtained from data of Fig. 75. Dashed curve: empirical representation of typical Kondo disorder behaviour. Solid curve: quadrature sum of Kondo disorder and (constant) site disorder contributions; latter is chosen to fit low-$|K|$ data.

[MacLaughlin *et al.*, J. Phys.: Condens. Matter **8**, 9855 (1996)], with temperature an implicit parameter).[3]

It is clear that $|\delta K/K|$ is essentially independent of $|K|$, indicating that the linewidth arises from *f*-ion site disorder rather than Kondo disorder. For comparison the dashed curve in Fig. 76 is a crude empirical representation of the behaviour found in systems in which Kondo disorder is the only significant broadening mechanism [*op. cit.*], where $|\delta K/K|$ varies roughly as $|K|^b$ with $b = 1.3$–1.6. Although the high-$|K|$ points appear to be consistent with the dashed curve, the dominant broadening mechanism is clearly site disorder, and one would expect linewidth contributions from both it and Kondo disorder. This is represented by the solid curve in Fig. 76, calculated assuming the broadening mechanisms are statistically independent and add in quadrature, which clearly overestimates $|\delta K/K|$ for large values of $|K|$. The small upturn in the data at large $|K|$ is suggestive of some degree of Kondo disorder, but it is not enough to account for the NFL properties of $Th_{0.7}U_{0.3}Pd_2Al_3$. We conclude that in this alloy Kondo disorder is not an important source of NFL behaviour, which must therefore be due to some other mechanism.

Experiment 791
Electronic structure and dynamics of charged muonium centres in semiconductors
(K.H. Chow, Lehigh; R.F. Kiefl, UBC; B. Hitti, TRIUMF)

There has been extensive experimental and theoretical work on atomic hydrogen in the elemental semiconductors. The theoretical calculations in Si are still considered the best understood of all the semiconductors. However, as in all other semiconductors, experimental information on the electronic structure and the dynamics mostly comes indirectly from the study of muonium.

Three distinct muonium signals (a diamagnetic and two paramagnetic) are observed in many semiconductors such as Si. The diamagnetic signal is due to a centre with no unpaired electronic spin and associated hyperfine interactions. Hence, information on the structure and dynamics of the diamagnetic centre is more difficult to obtain than for paramagnetic muonium since it relies on studying the much weaker muon-nuclear magnetic dipolar interaction.

A heavily-doped *p*-type Si:B $\approx 10^{19}$ cm^3 sample in which the full diamagnetic fraction is detected is used in this experiment. The two likely possibilities for the location of the muon when it is implanted into *p*-type Si are (1) near the BC (bond-centre) position with two Si nearest neighbours, i.e. isolated centre and (2) the BC position, complexed with an interstitial dopant atom. Detailed information on these states would further the understanding of the electronic structure and dynamics of hydrogen and muonium in Si.

The most likely state at low temperatures is the isolated μ^+ centre. The ability to study this centre is based on detection of the dipolar couplings with the Si^{29}. These nuclei only make up a small fraction of an otherwise essentially "invisible" spin-zero lattice. Si^{29} has a spin of 1/2 and a natural abundance of 4.7%. In order to increase the sensitivity of the experiment we use *time-integral* mode where there is no rate limitation. The experiment therefore consists of longitudinal magnetic field scans of the integrated polarization at selected temperatures. At magnetic fields which are low compared to the dipolar interaction, there will be a loss in the integrated asymmetry because the muon polarization decays. However, when the applied magnetic field is significantly greater than the dipolar interaction, the polarization is quenched and the integrated asymmetry will be fully recovered. In Fig. 77 we show the normalized asymmetry measured in the Si:B sample at room temperature with an applied transverse magnetic field of 1.5 G and after the field is removed. This clearly demonstrates the sensitivity of this technique to small fields. In Fig. 78 we compare the signal at 9 K and at 295 K. Note the increase in the amplitude of the signal at low temperature which we attribute to the Si^{29} nuclear dipolar interaction.

[3]For convenience the absolute values are plotted, since from Fig. 75(a) the shift (not corrected for Lorentz and demagnetizing fields) is negative.

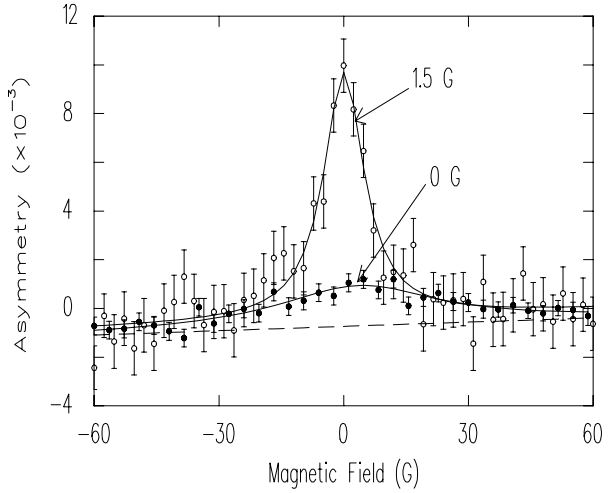

Fig. 77. The "zero-crossing" signal measured in Si:B at room temperature with an applied transverse magnetic field of 1.5 G and after the field is removed.

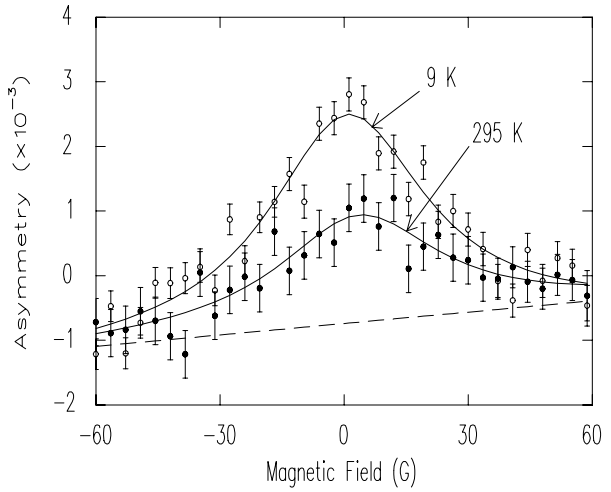

Fig. 78. Comparison of the signal in Si:B at 9 K and 295 K.

The method described above is novel and most likely the only way to study the diamagnetic centres is these important semiconductors.

Experiment 804
Muonium in gallium nitride
(R.L. Lichti, Texas Tech.)

Gallium nitride is the most important and best characterized of the wide bandgap group-III nitrides. These materials are presently being developed for blue and UV optical device applications. Hydrogen is an important impurity in the nitrides and passivates p-type dopants in as grown films requiring a high temperature anneal to release the bound H and activate the acceptors. As in more traditional semiconducting materials, investigation of muonium impurities by various μSR techniques provides one of the very few methods capable of yielding experimental information on isolated hydrogen defect states. Muonium is known to have very similar static properties to the analogous isolated hydrogen defect centres and, as demonstrated most convincingly in silicon, the dynamic features are at least qualitatively transferable [see eg. Lichti *et al.*, Mater. Sci. Forum **196-201**, 831 (1995); or Lichti, Phil. Trans. **A350**, 323 (1995)].

We have recently examined both a powdered sample of GaN and a *c*-axis oriented film of nominally undoped GaN to characterize the muonium centres formed. The powdered sample showed a single diamagnetic Mu state which exhibited hopping motion above roughly 550 K, with no other dynamic features present up to 800 K. Room temperature data from this sample also showed that quadrupolar level-crossing resonance (QLCR) measurements from which detailed local structural information can be obtained are feasible in a suitable GaN sample. The powder pattern QLCR spectrum had a large amplitude and clearly indicated that the diamagnetic Mu centre in that sample resides close to a Ga atom, but yielded no additional details. The QLCR data on the oriented film displayed the same Ga-related features and suggested a multi-line spectrum for each Ga isotope. The film which was studied initially was quite thin by μSR standards and only about 30% of the muons could be stopped in the GaN film, thus we were unable to cleanly separate signals from the GaN film from those due to the sapphire substrate and Ag mask. The main goal for the initial time allocated to Expt. 804 was to obtain a sufficiently detailed QLCR spectra from the best available GaN sample so that a detailed structural model for the observed diamagnetic muonium centre could be determined.

The two GaN samples examined previously were both nominally undoped, but are n-type due to a common unidentified impurity or native defect. Based on this information and muonium behaviour in other semiconductors, the observed diamagnetic centre was tentatively identified as Mu^-. Theoretical models place the Mu^- location at a gallium antibonding (AB_{Ga}) site, i.e. attached to a Ga atom directly opposite to a Ga–N bond [Estreicher and Boucher, in GaN and Related Materials, ed. S. Pearton (Gordon and Breach, 1996); Van de Walle, 19th Int. Conf. on Defects in Semiconductors, Aviero, July, 1997 (Mater. Sci. Forum, in press)].

In the GaN Wurtzite structure there are two inequivalent AB sites associated with each Ga atom with the muon "backbonded" opposite the two different Ga–N bonds: one site along the *c*-axis and the second at approximately 70° to the *c*-axis. This second site is expected to have a lower energy based on the positions of nearby host atoms; the site along the *c*-axis is much more confined. However, the QLCR spectra from the

oriented film showed a single strong resonance per Ga isotope which implies that the Mu–Ga direction is parallel to **c**. There were also suggestions of much weaker lines on either side of the strong resonances. One of the questions we sought to answer in the current experiment is whether these weaker features represent a second site or whether they could be assigned to the three additional Ga atoms which are either 2nd or 3rd neighbours to Mu^- depending on details of the local lattice distortion.

The sample used in the present experiment was a thick film prepared by HVPE methods (sample prepared by R. Molnar, MIT Lincoln Labs). It is a highly *c*-axis oriented film with a thickness of greater than 100 μm. The surface was rough, containing numerous hexagonal features such that the thickness approached 200 μm in some regions. These surface features do not affect the investigated muonium states since the muons are implanted much deeper into the film. The sample is nominally undoped with n-type characteristics typical of GaN and has an electron concentration in the mid 10^{16} cm^{-3} range.

Detailed QLCR spectra for Mu^-

Figure 79 displays a high statistics QLCR spectrum obtained on the thick film GaN sample. A linear background and the typical resonance due to state mixing at zero magnetic field have been removed from the raw data in preparing this figure, thus leaving only the QLCR features. As is immediately visible, the spectra contain two strong features each having a shoulder on the high field side. The ratio of field positions of the main peaks near 100 and 160 G closely matches the ratio of quadrupole moments for the two gallium isotopes, $Q(^{69}Ga)/Q(^{71}Ga) = 1.589$. This is a very clear indication that these spectral features should be assigned to interactions with gallium. There are additional hints of very weak structure on the low field side of each of these main lines. In initial attempts to fit this spectra to separate lines it became obvious that the large peaks are not symmetric, implying an additional unresolved line within each main peak in addition to the visible shoulder. Since there should be two lines associated with any angle other than zero between the applied field and the Ga–Mu direction, three lines were used to fit the spectrum from each Ga isotope. Because of the number of parameters and the lack of clean separation, a single linewidth was used within each three-line feature. The six lines shown in Fig. 79 are the result of a preliminary fit using this approach. These spectra clearly come from two different Ga–Mu directions; however, that does not distinguish between alternative explanations of two types of Ga atoms for a single site and two separate sites for Mu^-.

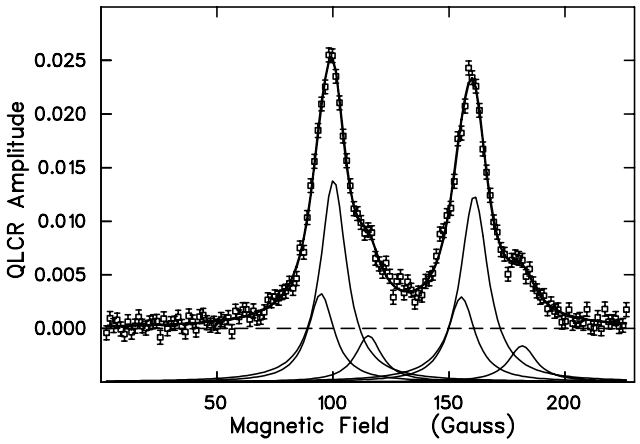

Fig. 79. QLCR spectra for the diamagnetic Mu centre in a thick *c*-axis oriented GaN film which is n-type in the mid-10^{16} cm^{-3} range. The fitted lines suggest two separate sites, each with the muon bound to a Ga atom.

The previously investigated Mu^- centre in GaAs can provide some useful information to help sort out such questions. As a direct comparison we examined the Mu^- QLCR spectrum in heavily doped n-type GaAs for fields applied along the $\langle 111 \rangle$ crystallographic direction. We have shown that the Mu^- site in GaAs is effectively centered at a symmetrically distorted T_{Ga} location within the zincblende structure [Chow *et al.*, Phys. Rev. **B51**, 14762 (1995)]. For the above experimental situation, each of the four Ga neighbours are equidistant, with one Ga–Mu direction parallel to the field and three at 70°. The GaAs spectrum matches a simulation for this structure quite closely, differing very slightly only in the relative intensity for the 0° and 70° features. For the symmetric structure of Mu^- in GaAs the electric field gradients at each Ga atom are also equivalent, thus the line positions reflect only a difference in Ga–Mu direction with respect to the magnetic field.

There are a number of differences in the QLCR spectra from GaAs and GaN which provide clues to the differences in the structure of the Mu^- centres. The most notable is that the intensity of the lines for GaN are roughly six to seven times those for GaAs. This implies a stronger dipolar coupling in GaN, which in turn indicates a smaller Mu–Ga distance. In the spectra from GaN shown in Fig. 79, the secondary lines have a relative intensity close to that expected for 70° but the positions are shifted to higher fields with respect to the central line compared to the GaAs spectrum implying a larger electric field gradient than for the more intense 0° line. For a single-site model one would naively expect a weaker field gradient for the three Ga atoms not strongly bound to Mu compared to that for the primary Ga atom in the AB_{Ga} structure. The net intensity in the doublet feature is also

only about 2/3 what would be expected if the dipolar coupling is similar for two types of Ga atoms within a single site. This later result could simply reflect the non-symmetric distortions expected for an AB_{Ga} site oriented along the *c*-axis. However, one additional observation appears to favour a two-site explanation. We also took a spectrum for a combination of all the oriented film samples. In this case the relative intensities of the central line and the doublet feature were different from that shown in Fig. 79, suggesting two sites with different relative populations in the two films.

Taken together the implications from these comparisons favour two separate Mu^- sites with the stronger spectral features coming only from the primary Ga atom which has Mu "backbonded" opposite the a Ga–N bond. The hint of very small doublet features at lower fields may then come from the more distant Ga atoms associated with one of these sites; however, it is unlikely that we will be able to determine the site to which these very weak features belong. If we assume that the dipolar coupling between the muon and Ga are the same for the two separate sites, then the relative intensities of the central line and related doublet from a single Ga isotope would imply that there is approximately a 2 to 1 site occupancy ratio with the 70° site favoured. We note that a very recent calculation for a negatively charged hydrogen or muonium centre in the GaN Wurtzite structure, performed at the approximate *ab initio* level (PRDDO), shows that both AB_{Ga} sites are a local minimum in the potential energy surface with the one oriented along the *c*-axis being metastable with a large barrier to migration into the more stable 70° site [Estreicher, private communication.] These calculations also show substantial structural rearrangement, particularly for the more confined metastable location.

Relaxation data for Mu^- in GaN

We have also examined the muon spin relaxation functions associated with the Mu^- centre in GaN for both transverse field (TF) and zero field (ZF) conditions. The initial reason for these studies in the thick film was to confirm that the motional behaviour previously observed in the powdered sample was general. For these measurements the sample was mounted in a furnace capable of reaching 1000 K or higher, and several layers of Ta foil were used as degrader to insure that very few muons reached the sapphire substrate. Above room temperature the metal foils give essentially a zero relaxation rate in both TF and ZF and can thus be separated from any relaxing signal related to Mu^- or any other Mu state in the GaN film.

An important initial observation is that there was a missing fraction in the TF-μSR data, suggesting that either some of the muons still reached the substrate or that there is a neutral muonium centre in this GaN sample. At higher temperatures the transverse relaxation rate increased rather than decreasing in the typical signature of motional narrowing as was observed in the earlier data from powdered GaN. These transverse relaxation rates are shown in Fig. 80. The general features displayed by these data are those normally associated with a muonium charge cycle [Chow *et al.*, Phys. Rev. **B47**, 16004 (1993)].

The zero field data are also somewhat different than those from the powdered sample which implied motion of the Mu^- centre. Because the zero field data require more extensive analysis they will only be described qualitatively here. There are two relaxing signals in zero field, one of which roughly follows that in the powdered sample up to about 700 K. The relative amplitudes of these two signals, and a third non-relaxing contribution appear to approximately reflect the missing fraction, the relaxing signal, and the non-relaxing signal seen in TF-μSR. We can thus assign the non-relaxing fractions to muons stopped in the metal foils and sample holder, and the TF relaxing fraction and the weakly relaxing ZF fraction to Mu^- in GaN. The additional fast relaxing ZF component at lower temperatures, up to about 600 K, corresponds to the missing TF fraction and appears to be a Mu^0 state, although we have not yet fully demonstrated that it comes from GaN. The fast ZF rate constant diverges at 600 K suggesting a transition, perhaps ionization of the Mu^0 state. The slower ZF rate was initially analyzed using a dynamic Kubo-Toyabe function with the expectation that the resulting hop rate would follow the results from the powdered GaN sample. Up to

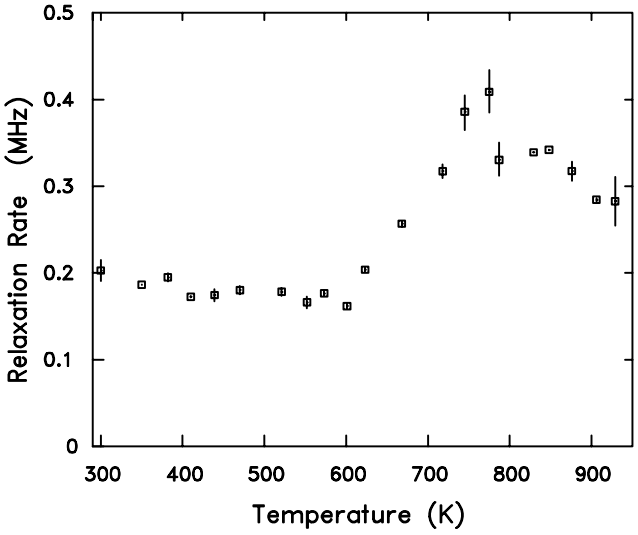

Fig. 80. Temperature dependence of the transverse field μSR relaxation rates for the negatively charged muonium centre in a thick *c*-axis oriented film of GaN. These data suggest a muonium charge cycle above 600 K.

roughly 700 K they are similar but above that temperature there are significant deviations from the earlier results.

In total, the relaxation data on the current GaN sample suggest that a neutral muonium centre may exist in GaN for n-type concentrations in the range of 10^{16} cm^{-3}, and that near 600 K this state undergoes a transition. Further work is needed to confirm that this signal is actually from the Gan film. However, the 600 K onset of features which seem to be from a muonium charge cycle, as shown in Fig. 80, is definitely from GaN, and thus lends support for such a conclusion. The differences in data from the thick film and powdered samples are probably due to a higher n-type concentration in the (uncharacterized) powdered GaN. The data discussed here represent the very early stages in our investigation of muonium centres in GaN and require more analysis and additional experiments before these preliminary conclusions can be more firmly established.

In conclusion, we have obtained high-statistics QLCR spectra for Mu^- in a thick *c*-axis oriented n-type GaN film and have examined the muon spin relaxation functions in both transverse and zero fields. The QLCR spectra clearly show interactions with the two Ga isotopes but have no verifiable feature which could be assigned to interactions with nitrogen. These spectra imply two separate Mu^- sites consistent with theoretical results showing local minima for Mu^- at the two inequivalent AB_{Ga} locations for the Wurtzite GaN structure. The relaxation results in the thick film yield qualitatively different dynamics from those inferred from earlier measurements on finely powdered GaN. The present data are most consistent with a muonium charge cycle above 600 K while the data from the powdered sample implied motion of the Mu^- centre. These differences may very well be due to significantly different n-type concentrations for the two samples. We plan to continue investigations of the muonium states and dynamics in GaN with special attention to semi-insulating and p-type material as sufficiently thick films or single crystals become available.